Jéssica Cândido Soares

Bachelor in Biochemistry

Insights into determinants of the activity of the flavodiiron NO reductase from *Escherichia coli*

Dissertation to obtain the Master's degree in Biochemistry for Health

Supervisor: Prof. Dr. Miguel Teixeira, Full Professor, ITQB-NOVA

Co-supervisor: Dr. Filipe Folgosa, Investigator, ITQB-NOVA

November 2020

Jéssica Cândido Soares

Bachelor in Biochemistry

Insights into determinants of the activity of the flavodiiron NO reductase from *Escherichia coli*

Dissertation to obtain the Master's degree in Biochemistry for Health

Supervisor: Prof. Dr. Miguel Teixeira, Full Professor, ITQB-NOVA

Co-supervisor: Dr. Filipe Folgosa, Investigator, ITQB-NOVA

November 2020

Insights into determinants of the activity of the flavodiiron NO reductase from Escherichia coli

Agradecimentos

Muitas pessoas para além de mim contribuíram para esta tese. Gostaria de tentar expressar a minha gratidão através deste pequeno texto.

Aos meus colegas de laboratório: Diogo, Maria, Silviya, Bruno e Susana – obrigada por todo o apoio técnico, trocas de informações e boas risadas no lab.

Ao meu coorientador, Dr. Filipe Folgosa, um obrigado não é suficiente por tudo o que fizeste por mim durante este ano. Obrigada por me teres ensinado (pacientemente, na maior parte do tempo) sobre ciência, mas também sobre aviões, espiões e outros assuntos interessantes da vida. Obrigada por esclareceres todas as minhas dúvidas (sempre!), por todas as risadas que me proporcionaste e também por perceberes que a minha mente funciona num registo ligeiramente diferente das outras mentes.

Ao Prof. Miguel Teixeira obrigada por ter estado sempre presente e disponível para esclarecer as minhas dúvidas, por todas as oportunidades que me concedeu e pelo grande voto de confiança que depositou em mim.

Aos meus amigos do ITQB: Marta, Anaísa, Tiago, Diogo, Carolina e Rodrigo – obrigada por fazerem dos meus dias os mais engraçados e cómicos de sempre. Obrigada por todas as pausas na varanda, todos os almoços e lanches, todas as conversas que iam de política aos vídeos cómicos do Youtube, todos os enigmas e por toda a ajuda intelectual no âmbito da tese. À minha amiga Marta, especialmente, obrigada por teres estado lá para tudo!

Aos meus amigos Nuno, Ana e Carlos obrigada pela vossa amizade, incentivo, bons jantares e inspirações para as minhas figuras da tese.

To my friends Val and Ish: I am really grateful for getting to know you. Thank you for all the English tips and time spent on the phone practising with me.

À professora Teresa Catarino que se tornou uma amiga, para além de minha professora e coordenadora do MBpS, muito obrigada pelas *endless* conversas de e-mail, sempre com uma ótima disposição independentemente do tema. Agradeço também por ter tornado a enzimologia algo tão leve e interessante e por me ter transmitido tão bem esse conhecimento. Foi muito útil na tese!

Não poderia deixar de incluir um agradecimento especial ao meu café de eleição, Full House, por todos os cafés, horas de eletricidade e internet oferecidas para que esta tese fosse concluída.

À minha amiga Mariana, não há palavras para descrever o tanto que contribuíste para esta tese, direta e indiretamente. Obrigada por toda a paciência e dedicação que sempre tiveste para comigo. Sem ti, este trabalho não teria sido possível de todo.

À minha mãe, um imenso e eterno obrigado porque sempre fez de tudo para que eu tivesse a melhor educação possível. Obrigada por todo o teu esforço, compromisso e dedicação para comigo, sem ti esta tese também não seria possível.

Agradeço também à Fundação para a Ciência e Tecnologia pelo suporte e financiamento através projeto PTDC/BBB-BQB/3135/2014 e ao TIMB3 por todas as oportunidades de aprendizagem; Ao ITQB um agradecimento especial por me ter proporcionado um excelente local de trabalho.

FCT Fundação para a Ciência e a Tecnologia

timb3

Resumo

As proteínas flavodiférricas (*flavodiiron proteins,* FDPs) formam uma família de metaloproteínas envolvidas na redução do oxigénio molecular e peróxido de hidrogénio a água e/ou a redução de óxido nítrico a óxido nitroso.

Análises bioinformáticas da estrutura primária das FDPs levaram à identificação de um motivo bastante conservado em FDPs da classe B (flavorubredoxinas, FlRd), relativamente perto do centro ativo. O presente trabalho laboratorial teve como objetivo estudar o papel desempenhado por duas serinas pertencentes a esse motivo numa FDP de *E.coli*. Para tal, dois mutantes, S33D e S34D, foram estudados e caracterizados de forma a determinar as implicações de tais mutações nas propriedades bioquímicas, cinéticas e espetroscópicas da enzima. A produção dos mutantes foi conseguida em *E. coli* BL21 (DE3) Gold e verificou-se que as características bioquímicas foram mantidas quase inalteradas.

As atividades das proteínas mutantes para a redução do O_2 e H_2O_2 mantiveram-se na mesma ordem de grandeza quando comparadas aos valores obtidos para a proteína nativa (atividade para o O_2: 1.61 ± 0.26 s^{-1}, 1.93 ± 0.37 s^{-1} e 1.89 ± 0.32 s^{-1}; atividade para o H_2O_2: 1.76 ± 0.04 s^{-1}, 1.56 ± 0.12 s^{-1} e 1.75 ± 0.31 s^{-1}, valores para FlRd nativa, S33D e S34D, respetivamente), enquanto que a atividade dos mutantes para a redução de NO foi claramente afetada, diminuindo para cerca de metade (11. 1 ± 1.1 s^{-1}, 5.4 ± 0.5 s^{-1} e 6.0 ± 0.4 s^{-1}, valores para FlRd nativa, S33D e S34D, respetivamente). A caracterização estrutural dos centros da rubredoxina e do centro catalítico diférrico foi conseguida por espetroscopia de ressonância paramagnética eletrónica (RPE).

Verificou-se que possivelmente ocorrem alterações estruturais quando as serinas são mutadas por aspartatos devido às diferentes propriedades físico-químicas de ambos os resíduos, contudo não foi possível obter nenhuma estrutura cristalográfica para nenhum dos dois mutantes. Pode concluir-se também, que o motivo onde se localizam as serinas em estudo é importante para a atividade de redução do óxido nítrico pela FDP de *E. coli.*

Palavras-chave: *Proteínas flavodiférricas; flavorubredoxina; cinética enzimática; ressonância paramagnética eletrónica*; *óxido nítrico*

Abstract

Flavodiiron proteins (FDPs) are a family of metalloproteins involved in the reduction of molecular oxygen and hydrogen peroxide to water and/or the reduction of nitric oxide to nitrous oxide.

Bioinformatic analysis of the primary structure of the FDPs led to the identification of a conserved motif in class B FDPs (flavorubredoxins, FlRd), that is relatively close to the active centre. The present experimental work aimed to study the role played by two serines present in this motif in an FDP from *E.coli*. Thus, two mutants, S33D and S34D, were studied and characterized in order to determine the implications of such mutations on the biochemical, kinetic and spectroscopic properties of the enzyme. The production of the mutants was achieved in *E. coli* BL21 (DE3) Gold and it was found that the biochemical characteristics were kept almost unchanged.

The activities of mutant proteins for the reduction of O_2 and H_2O_2 remained in the same order of magnitude when compared to the ones obtained for the wild type protein (activity for O_2: 1.61 ± 0.26 s^{-1}, 1.93 ± 0.37 s^{-1} and 1.89 ± 0.32 s^{-1}; activity for H_2O_2: 1.76 ± 0.04 s^{-1}, 1.56 ± 0.12 s^{-1} and 1.75 ± 0.31 s^{-1}, values for wild type protein, S33D and S34D, respectively), while mutants' activity for NO reduction was clearly affected, decreasing to about half (11. 1 ± 1.1 s^{-1}, 5.4 ± 0.5 s^{-1} and 6.0 ± 0.4 s^{-1}, values for wild type, S33D and S34D, respectively). The structural characterization of the rubredoxin centre and the diiron catalytic centre was achieved by electronic paramagnetic resonance (EPR) spectroscopy.

Even though it was not possible to obtain any crystallographic structure for either mutant, it is possible to conclude that structural changes possibly occur when serines are mutated by aspartates due to their different physical and chemical properties. Also, the motif where the serines under study are located is important for the activity of nitric oxide reduction by the FDP from *E. coli.*

Keywords: *Flavodiiron proteins; flavorubredoxin; enzyme kinetic; electron paramagnetic resonance*; *nitric oxide.*

Symbols and abbreviations

FlRd – Flavorubredoxin

FDP – Flavodiiron Protein

E. coli *– Escherichia coli*

ROS – Reactive Oxygen Species

RNS – Reactive Nitrogen Species

SDS-PAGE – Sodium Dodecyl Sulphate-PolyAcrylamide Gel Electrophoresis

Ser33 – Serine 33 from FlRd from *E. coli*

Ser34 – Serine 34 from FlRd from *E. coli*

CD – Circular Dichroism

EPR – Electron Paramagnetic Resonance

Tris – Tris(hydroxymethyl)aminomethane

IPTG – Isopropyl β-D-1-thiogalactopyranoside

Table of contents

Figure index

Table and appendices index

1. Introduction

1.1. Oxygen and reactive oxygen species

Nowadays, an important part of life on Earth is based on a well-oxygenated ocean-atmosphere system and depends on the availability of free molecular oxygen (O_2). Oxygen's atmospheric concentrations first rose to significant levels after the so-called Great Oxidation Event (GOE), roughly 2.5 billion years ago, and eventually stabilised at around 21%, in a process intimately related to the evolution of photosynthesis performed by cyanobacteria. [1]

Life on Earth was then drastically changed by the establishment of an oxidizing environment and the organisms that were naturally present in environments that remained anaerobic had greater chances of surviving. However, throughout the evolution, organisms began to acquire new mechanisms to cope with the exposure to oxygen. Despite greatly changing Earth's early environment, the appreciable presence of oxygen in the atmosphere allowed for its introduction in respiration as the final electron acceptor, leading to the most efficient process for energy conservation currently known: the oxidative phosphorylation, through which adenosine triphosphate (ATP) is produced to be used in the cell as the main energy carrier. [2] Molecular oxygen is an extremely electronegative molecule and a potent oxidant agent (its reduction potential to water is E°'= +0.82 V at pH 7). [3]

Although oxygen plays a key role in aerobic metabolism, either by itself or via some of its reduction products, that include very reactive species (generically designated as reactive oxygen species, ROS), can be extremely harmful to the cell. The type of ROS formed is dependent on the number of electrons used in O_2 reduction as shown in Figure 1.

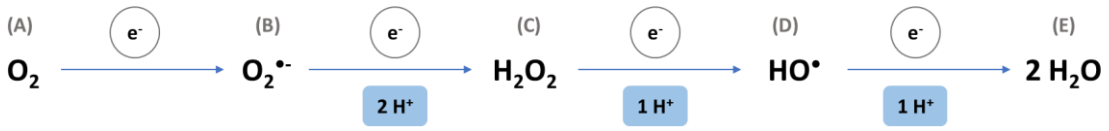

Figure 1 – **Reduction of molecular oxygen by consecutive one-electron reductions**. **(A)** Molecular oxygen; **(B)** Superoxide anion radical; **(C)** Hydrogen peroxide; **(D)** Hydroxyl radical; **(E)** Water.

Reactive oxygen species can be radicals, such as the superoxide anion (Figure 1, B) or the hydroxyl radical (Figure 1, D), that possess unpaired electrons, or non-radical, such as hydrogen peroxide (Figure 1, C). Non-radical ROS can be transformed into radical ROS in the presence of transition metals, namely iron, as in H_2O_2 conversion to $OH^{\bullet}$ through the Fenton reaction (Equations 1 and 2). [4]

$$H_2O_2 + Fe^{2+} \rightarrow Fe^{3+} + HO^- + HO^\bullet$$ Equation 1

$$Fe^{3+} + H_2O_2 \rightarrow Fe^{2+} + HOO^\bullet + H^+$$ Equation 2

Oxygen and its derived species react with a plethora of vital molecules such as proteins, cofactors and metallic centres, leading to their inactivation and impairment of key metabolic pathways, being intimately linked to a variety of human diseases, such as cancer, chronic inflammation and numerous age-related diseases. [5] Some components of the higher organisms' immune system also use hydrogen peroxide and superoxide to fight pathogens and they are essential in cell growth and differentiation. [6] Indeed, it is now clear that the generation of ROS is of enormous relevance to the innate immune system. According to Yang and co-workers [7], the main source of ROS in the immune system is a membrane-bound NADPH oxidase (NOX2) that generates a large amount of superoxide anion, that later undergoes dismutation to hydrogen peroxide and oxygen by superoxide dismutase (SOD).

1.2. Nitric oxide

Besides oxygen and reactive oxygen species, another diatomic and radical molecule plays an important role in the innate immune system: the nitric oxide (NO) molecule. According to previous studies, upon infection or inflammation higher amounts of nitrogen products can be found in the urine [8] and the plasma [5]. Those studies provided strong evidence that nitric oxide plays a main role in the innate immune system and allowed for the understanding of the properties of NO and other NO-related molecules in that system.

In the human body, nitric oxide production is mainly a function of the Nitric Oxide Synthase (NOS) enzyme, that catalyses the conversion of L-arginine and molecular oxygen to L-citrulline and NO, necessary in host defence and vascular homeostasis, using 1.5 molecules of NADPH and 2 molecules of oxygen. This enzyme has three isoforms: neuronal NOS (nNOS or NOS1) and endothelial NOS (eNOS or NOS3) that are constitutively synthesised and are calcium-dependent; and inducible NOS (iNOS or NOS2), associated with the innate immune system, that is inducible and calcium-independent. The regulation of NO production is intimately related to the availability of its precursors and the activity and coordination between the three isoforms of NOS, but it is also influenced by non-enzymatic pathways that depend on the oxygen pressure, pH and nitrate/nitrite availability. The presence of iNOS in macrophages has been confirmed for humans, horse, cow, goat, sheep, rat, mouse, and chicken and is regulated by cytokines and microbial products, that will activate NO production and its redox pathways, inhibiting the growth of pathogens. [8]

With a molecular mass of 30 Da, NO is one of the smallest signalling molecules currently known. It is a relatively nonreactive molecule that has as main targets transition metals incorporated in haems, non-haemic iron and free radicals, as well as thiols, but it can also be activated upon reaction with superoxide to generate other reactive nitrogen species (RNS), namely peroxynitrite.[9]

1.3. ROS and RNS in the innate immune system

As a part of the innate immune system, the NO molecule and the RNS can act in the organism separately from ROS or combined with it, but the role played by each molecule is dependent on which, NO or superoxide, is the starting molecule in the redox pathway. The tendency for following preferably a certain pathway instead of another is highly dependent on the microenvironment in which the molecule of NO is present. [5, 8] In the presence of signals determining the presence of pathogens in the phagocytic cells, there is a burst of superoxide anion production by the membrane NAPDH phagocyte oxidase (NOX) that leads to the generation of oxidative stress inside the phagosomes causing the damage of pathogen's biomolecules. [5]

Due to its high lipophilicity, NO possesses higher mobility across membranes and cells comparatively to superoxide, a charged molecule restrained to specific compartments inside the cell. Besides that, the iNOS protein can be found in the cytosol and bound to the phagosome membrane allowing for the production of NO in less restricted zones of the cell, comparatively to superoxide anion. Thus, in case the biomolecule from the pathogen is not in a superoxide-rich environment, it can still be damaged if in the presence of NO, that is more widespread inside the cell than the ROS. [5]

Since the combination of NO with ROS leads to the formation of RNS, the restriction in superoxide production zones inside the cell makes the presence of superoxide the limiting step for the formation of RNS. [10] Thus, when the NO molecule encounters superoxide-rich environments there is a rapid production of RNS such as $ONOO^-$, that reacts rapidly with carbon dioxide (CO_2) forming nitrosoperoxocarboxylate (CO_2-$ONOO^-$), an unstable intermediate that is readily converted to nitrous oxide (N_2O) and dinitrogen trioxide (N_2O_3) – a nitrosating agent. [9] Other reactive species can also be formed, such as hypochlorous acid (HOCl), nitrosothiols (RSNO) and even singlet oxygen ($^1O_2$) under specific conditions. [5, 6, 11] Even though each protein, NOX and iNOS, catalyse a specific reaction producing superoxide and NO, respectively, there is a complex combination of both pathways that makes it a challenge to describe them separately and without taking into consideration the high synchronicity of the process. The summary of the main interactions observed is shown in Figure 2.

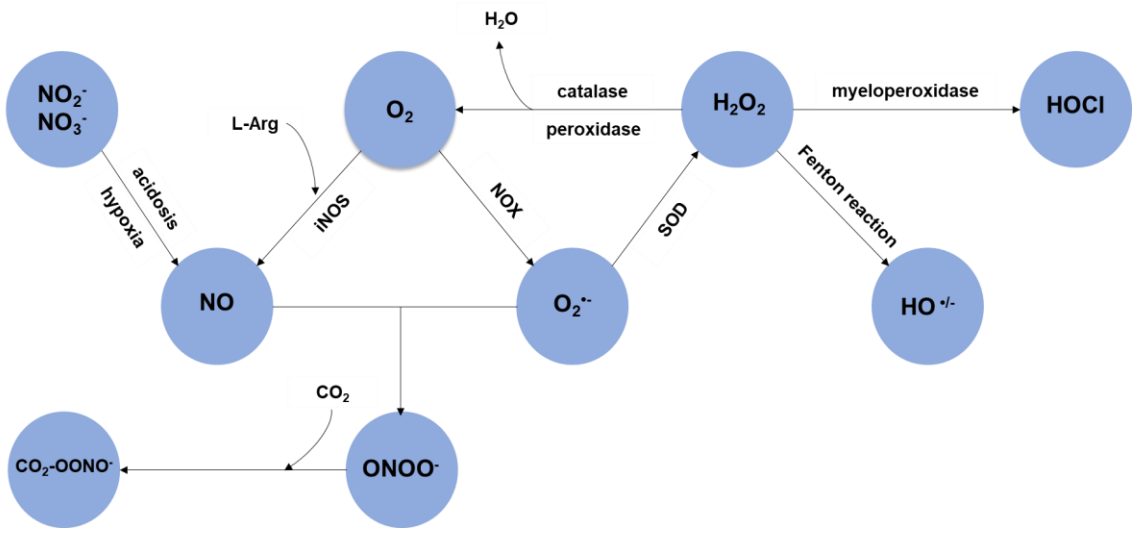

Figure 2 – General view of the possible interactions between molecular oxygen, nitric oxide, and their by-products in the human body. These interactions are highly organised in a complex pathway dependent on the microenvironment, concentrations of each species and nature of the signal received by the cells.

1.4. Oxygen and NO scavenging systems

While higher organisms evolved towards using oxygen by-products and nitric oxide as a primary response of the innate immune system and as signalling molecules, microbes' evolution occurred towards the development of new mechanisms to cope with the new challenges presented by their hosts. By producing proteins that are capable of scavenging harmful molecules, such as oxygen, NO and their by-products, bacteria become resistant and can survive for a longer time inside the host. [12]

As soon as a bacterium enters the host, its stress sensors begin to activate the signalling process to adapt and/or fight the new obstacles imposed by the host. One of these obstacles is exactly the generation of oxidative and nitrosative stress mentioned in the previous section. The almost ubiquitous presence of oxygen and ROS scavenging mechanisms in all organisms reveals the clear need to deal with those molecules. [10, 11]

Starting from the sensors of oxidative and nitrosative stress, Vasquez-Torres [12] describes a set of proteins with strategically positioned cysteines that, due to their versatile redox state, are appropriate to function as sensors and initiate signalling cascades through redox induced conformational changes, working as transcriptional factors for the transcription of ROS- and RNS-scavenging proteins. According to the sensor that is activated, the cell can do the recruitment of the appropriate machinery to cope with the threat presented. Aside from the cysteine-based sensors, other proteins such as the Fumarate:nitrate regulator (FNR) [13] and NorR [14] were also described as NO sensors, the last one being responsible for the activation of *norVW* genes transcription, leading to the production of *Escherichia coli* FDP and FDP-reductase.

Besides the transcriptional-regulating proteins, there are several reported ROS scavenging mechanisms. Some of the best studied are SODs, that catalyse the dismutation of superoxide to oxygen and hydrogen peroxide, and catalase, that converts the hydrogen peroxide molecule into molecular oxygen and water. Proteins with peroxidase activity are also part of the ROS scavenging system by oxidizing several substrates and reducing hydrogen peroxide to water. [10, 11] Other proteins, such as the alternative oxidase (AOX), and its homologous proteins in bacteria, provide an escape route for electrons, decreasing the generation of oxidative stress inside the cells and contributing not for the scavenge process itself, but for the decrease of ROS production. [15,16]

It is also known that NO and RNS scavenging are performed by enzymes such as S-nitrosoglutathione reductase (GSNOR), that control the levels of S-nitrosoglutathione and is involved in the conservation of the balanced levels of reactive nitrogen species [17], NO reductases, that catalyse the reduction of NO to nitrous oxide (N_2O), and peroxynitrite reductases that reduce peroxynitrite to nitrite. [18]

Molecular oxygen can be fully reduced to water not only by membrane-bound oxygen reductases, such as haem-copper reductases and cytochrome *bd*, but also by the cytoplasmatic Flavodiiron Proteins (FDPs), which will be the subject of this thesis. [19]

1.5. Flavodiiron proteins – FDPs

Flavodiiron proteins were first described in 1993 by Chen and co-workers [19] while studying the oxygen resistance observed for the sulphate reducing bacterium *Desulfovibrio gigas*. It was found that a protein, named rubredoxin:oxygen oxidoreductase (ROO) at that time, was able to catalyse the reduction of molecular oxygen to water, using NADH as electron donor and requiring an NADH:rubredoxin oxidoreductase and a rubredoxin for electron transfer. Since then, homologous proteins were discovered in other species and the family of Flavodiiron proteins was found to play an important role in NO and oxygen detoxification mechanisms, in all life domains (Bacteria, Eukarya and Archaea). [20-22]

This family of proteins was named Flavodiiron proteins due to the presence of a common core composed by a diiron catalytic centre – in a metallo-β-lactamase like domain – followed by a flavodoxin-like domain, that harbours a non-covalently bound FMN, in the C-terminus. [20, 21]

These proteins, present in a variety of human pathogens, are particularly interesting since they constitute a mechanism of resistance against harmful molecules that hosts use to defend themselves from infection, as well as allowing anaerobes to resist to small amounts of oxygen,

also present in the host. FDPs catalyse the conversion of molecular oxygen to water and/or the conversion of nitric oxide to nitrous oxide [19, 23], as shown in Equations 3 and 4:

$$O_2 + 4\,e^- + 4\,H^+ \rightarrow 2\,H_2O \qquad \text{Equation 3}$$

$$2\,NO + 2\,e^- + 2\,H^+ \rightarrow N_2O + H_2O \qquad \text{Equation 4}$$

Some FDPs present similar activities for both molecular oxygen and nitric oxide (e.g from sulphate reducing bacteria like *D. gigas* and *Desulfovibrio vulgaris*), while others are selective regarding their main substrate that can be either molecular oxygen (e.g from phototrophic organisms like *Synechocystis* or Clostridiales such as *Clostridioides difficile*) or NO (e.g from *E. coli*). Although the substrate preference in this family of proteins has been extensively studied, the reason for that preference was not completely clarified yet, being partially modulated by two amino acids near the active site (Residues 53 and 271 in *Entamoeba histolytica* FDP numbering). [24, 25]

Folgosa, Kint and co-workers [26,27] showed that, besides oxygen and NO reduction, FDPs are also capable of reducing hydrogen peroxide to water using two electrons, thus displaying hydrogen peroxide reductase activity.

1.5.1. Classes of FDPs

The current organisation of the FDP family comprises nine classes. Those classes contain at least the common flavodiiron core, that can be or not followed by other functional domains at the C-terminus (Figure 3).

The most widespread FDP is the class A one, that is also the simplest one being composed only by the flavodiiron core. This class is mostly found in anaerobes, and has been isolated from sulphate reducing bacteria (*D. gigas* and *D. vulgaris* [19]), methanogens (*Methanobrevibacter arboriphilus* [28] and *Methanothermobacter marburgensis* [29]), purple bacteria (*Rhodobacter capsulatus* [30]), pathogenic unicellular protists (*Trichomonas vaginalis* [31], *Giardia instestinalis* [32] and *Entamoeba histotlytica* [33]) and also from a few bacteria from the Firmicutes phylum (*Moorella thermoacetica* [34], *Clostridium acetobutylicum* and *Clostridium difficile* [27]).

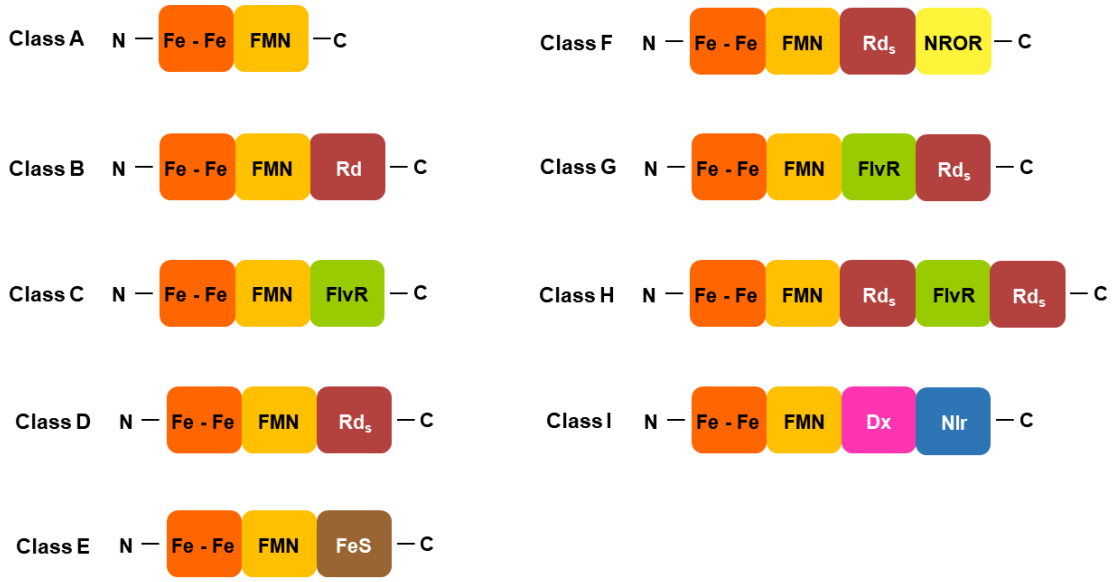

Figure 3 – C**urrent organisation of flavodiiron proteins in nine classes. Fe-Fe –** diiron centre; **FMN** – flavodoxin-like domain; **Rd –** Rubredoxin; **FlvR –** NAD(P)H:flavin oxidoreductase; **Rd$_s$ –** Short rubredoxin; **FeS** – Iron-sulphur cluster; **NROR** – NADH:rubredoxin oxidoreductase; **Dx** – Desulforedoxin-like domain; **Nlr –** Neelaredoxin-like domain. Adapted from Martins, M. C. et al.[21]

The Class B FDP, also named flavorubredoxin (FlRd), was firstly described in 1998 by Wasserfallen and co-workers [30] for the facultative anaerobe *E. coli*. According to their report, this protein would be composed by the common flavodiiron core fused to a rubredoxin-like domain. In 2002, Gomes and co-workers [23] reported the high activity of this protein for NO reduction, being established a new class of NO reductase from prokaryotes. This discovery showed that the Class B FDP from *E. coli* not only presented activity for NO reduction, but that NO was the preferred substrate, and having a negligible oxygen activity, this protein being then characterized as a bona fide NO reductase. Other FDPs' ability for NO reduction has been tested since then, and some FDPs have similar activities for NO or O_2 reduction. [21]

Class C FDPs were also first described in 1998 by Wasserfallen and co-workers [30], for the FDP from *Synechocystis sp*. PCC6803, a freshwater cyanobacterium. In their report, the presence of two flavin containing domains was mentioned, one belonging to the flavodiiron core and the other, present at the C-terminus, harbouring a FAD and similar to flavin reductases. In 2003, Helman and co-workers [36] described for the first time the involvement of this protein in oxygen photoreduction in cyanobacteria and, in 2015, Allahverdiyeva and co-workers [37] described the protective role this protein plays during the photosynthetic process in cyanobacteria. Class C FDPs are present in all oxygenic phototrophs, excluding angiosperms. [38]

Class F FDPs were first described in 2018, by Folgosa and co-workers [26], being a four domains complex FDP. In this class, the flavodiiron core is followed by a short-rubredoxin like domain, and an NADH:rubredoxin oxidoreductase-like domain. This protein does not require any other redox partner, being able to oxidise NADH with the NROR domain and transfer the electrons

within its domains, being described as a standalone protein, contrarily to Classes A and B FDPs. This class of proteins is mainly found in the phylum Firmicutes, namely in the Clostridiales order, but is also in pathogenic protozoa, such as *Tritrichomonas foetus* and *T. vaginalis*. [31]

There are no reported studies about the other FDPs' classes. Their domains and features were predicted based on amino acids sequence alignments and structural predictions. Class D FDPs appear to be similar to Class B FDPs having as extra domain a rubredoxin, but, in Class D FDPs, this domain is a short-rubredoxin (Rd_S), instead of the canonical rubredoxin-like present in Class B. Class E FDPs appear to possess an extra domain with a putative Fe-S cluster. Both Classes D and E were only found in Clostridiales genomes, from the Firmicutes phylum. Other classes were found in Firmicutes: – the Class G FDP –, that appears to be a fusion of Class C with one or two short-rubredoxin like domain (Rd_S), found mainly for the Lactobacillales, Clostridiales and Erysipelotrichia orders. For the Firmicutes phylum, Clostridiales order, the presence of Class H FDPs was also reported that present, besides the common core, a short-rubredoxin, followed by a flavin reductase-like, and by a second short-rubredoxin domain. [20]

Another Class of FDPs (Class I) was recently considered for the strict anaerobe *Anaerofustis stercorihominis*. This class seems to be a fusion of Class A FDP with a 2 Fe superoxide reductase (SOR), presenting two extra domains at the C-terminus that would correspond to centres I and II of SORs. [21]

1.5.2. The structure of FDPs

The flavodiiron proteins' common core is composed by a metallo-β-lactamase like domain, containing the catalytic diiron centre, and the flavodoxin-like domain, containing an FMN. This core is the minimal structural unit found in this family of proteins. The diiron domain is organized in an αββα pattern, composed of two inner β-sheets surrounded by two sets of three α-helices, while the flavodoxin-like domain is organised in a typical αβα flavodoxin fold of three parallel inner β-sheets surrounded by two sets of two α-helices. Interestingly, within a monomer both redox centres are at *ca.* 40 Å apart from each other, preventing electron transfer between them (Figure 4). [39, 40]

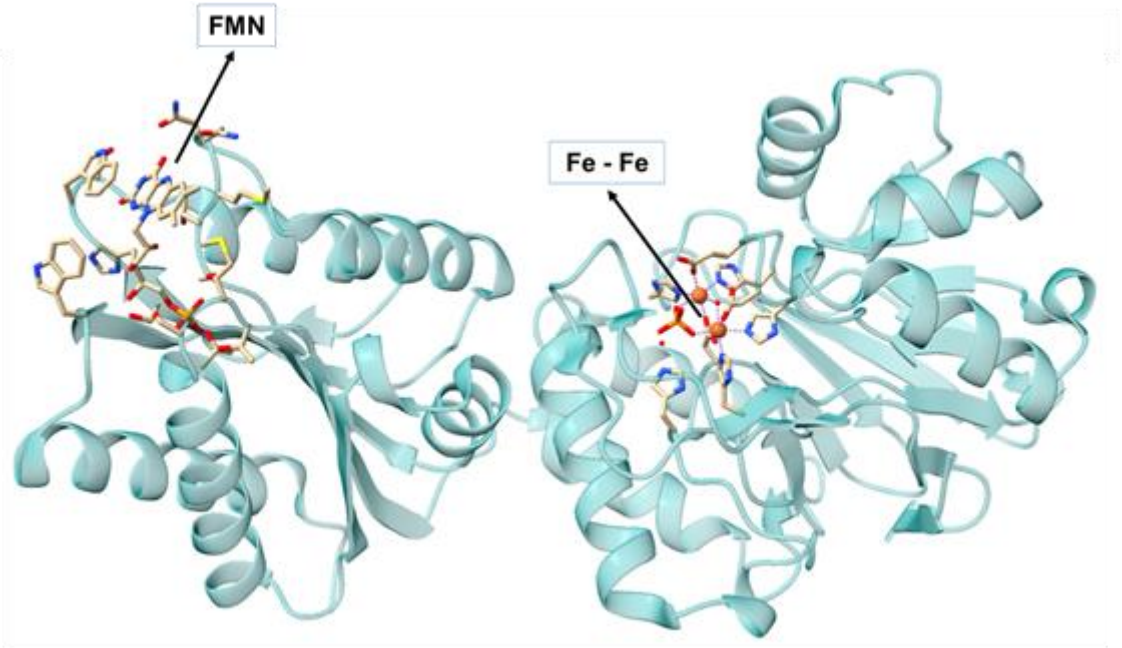

Figure 4 – **Cartoon representation of one FlRd monomer.** In this representation the diiron centre (Fe-Fe), the FMN and their corresponding ligands are represented as sticks and identified by the arrows. PDB code: 4D02. [40]

However, the spatial organisation of the monomers as a head-to-tail homodimer or as dimers of dimers (homotetramer), allows for the effective electron transfer between the FMN of one monomer and the diiron centre of the other monomer since these cofactors are then located at *ca.* 3.5 Å apart from each other (Figure 5).

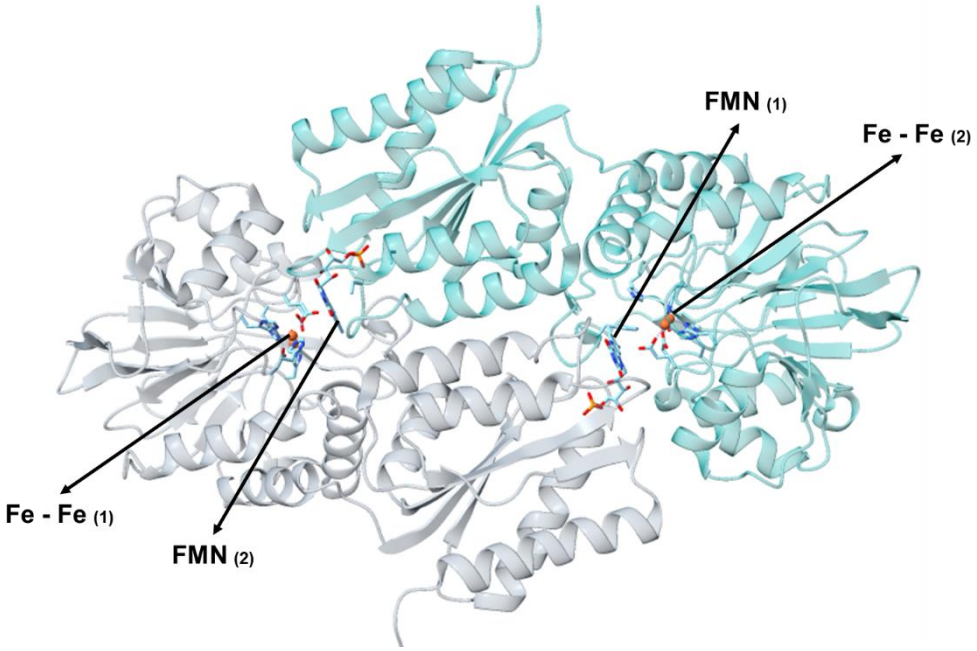

Figure 5 – Cartoon representation of the FlRd homodimer showing a head-to-tail spatial organisation. In this representation the monomers are coloured in grey (1) and light blue (2). (1) refers to one monomer, whereas (2) refers to the other monomer of the dimer. PDB code: 4D02. [40]

1.5.3. The electron transfer process

The intra and inter monomers' electron transfers in the FDP family are very complex due to the great diversity of C-terminal domains that are present in the nine classes of FDPs. Generally, the electron transfer pathway is initiated by the oxidation of NAD(P)H by an NAD(P)H oxidase which can be one of the domains of the FDP (Classes C, F and possibly H and G) [21, 26] or a redox partner (other classes). [19,30] Subsequently, electrons are transferred from the NAD(P)H oxidase to another domain, such as the rubredoxin-like (Class B) [30], short-rubredoxin-like (Classes D, F, G and H) [21, 26] or Fe-S clusters (Class E) [21], or to another redox partner such as rubredoxins as an independent protein (Class A) [19]. Then, electrons are transferred towards the flavodoxin-like domain, that later transfers the electrons to the diiron site of the other monomer of the dimer, where catalysis occurs. Electrons can also be transferred directly to the flavodoxin-like domain in some Class A FDPs having coenzyme F420 (characteristic of methanogens) [28] or ferredoxin (Fd) [41] as electron donor, instead of NAD(P)H. The general mechanism of electron transfer can be schematised as shown in Figure 6.

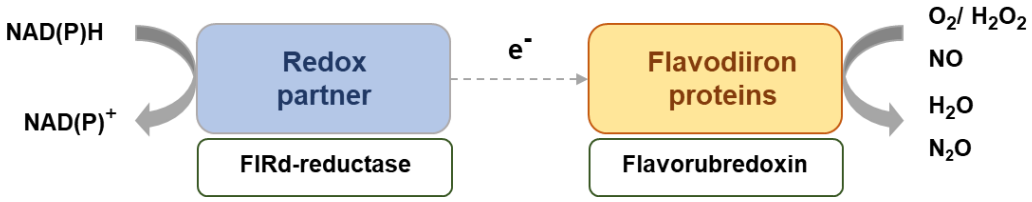

Figure 6 – **Schematic view of the general process of electron transfer proposed for the flavodiiron proteins.** The catalytic mechanism of FDPs requires an electron donor (usually NAD(P)H) and reduces water and hydrogen peroxide to water, and also nitric oxide to nitrous oxide. Represented in white boxes are the redox partner and FDP studied in this experimental work: FlRd-reductase and Flavorubredoxin, respectively.

1.5.4. The active site

The Fe-Fe centres are found on the interface between the two monomers of the dimer, their solvent exposure being limited by the presence of the FMN cofactors of the other monomer, caused by the dimerization. The iron atoms are designated proximal or distal according to their distance relative to the FMN cofactor. [39, 40]

The crystallographic structure of the FDP from *E. coli* shows, as was also observed for other FDPs, that each iron atom is penta-coordinated, having a distorted square pyramidal geometry, in the ferrous state and hexa-coordinated, showing a distorted octahedral geometry in the ferric state. The iron atoms were shown to be coordinated by a conserved group of amino acids, with a total of four imidazole and three carboxylate groups. Each iron atom is coordinated by two imidazole groups (belonging to histidine residues) and one carboxylate (belonging to glutamates or aspartates residues); a third carboxylate group coordinates both iron atoms. [40] Besides that, at least

one μ-OH bridge links the iron atoms. [34, 42] In the case of the *E. coli* FDP, that bridge is stabilised by a hydrogen bond with the remaining oxygen from the carboxylate that coordinates the distal iron atom, the distance between the two iron atoms being 3.4 and 3.8 Å, in the oxidised and reduced states, respectively. The remaining oxygen from the carboxylate that coordinates the proximal iron is found to be very close to the FMN (3.5 Å from the C8 methyl group of the isoalloxazine ring to the non-bonding carboxylate oxygen) (Figure 7). [21, 40]

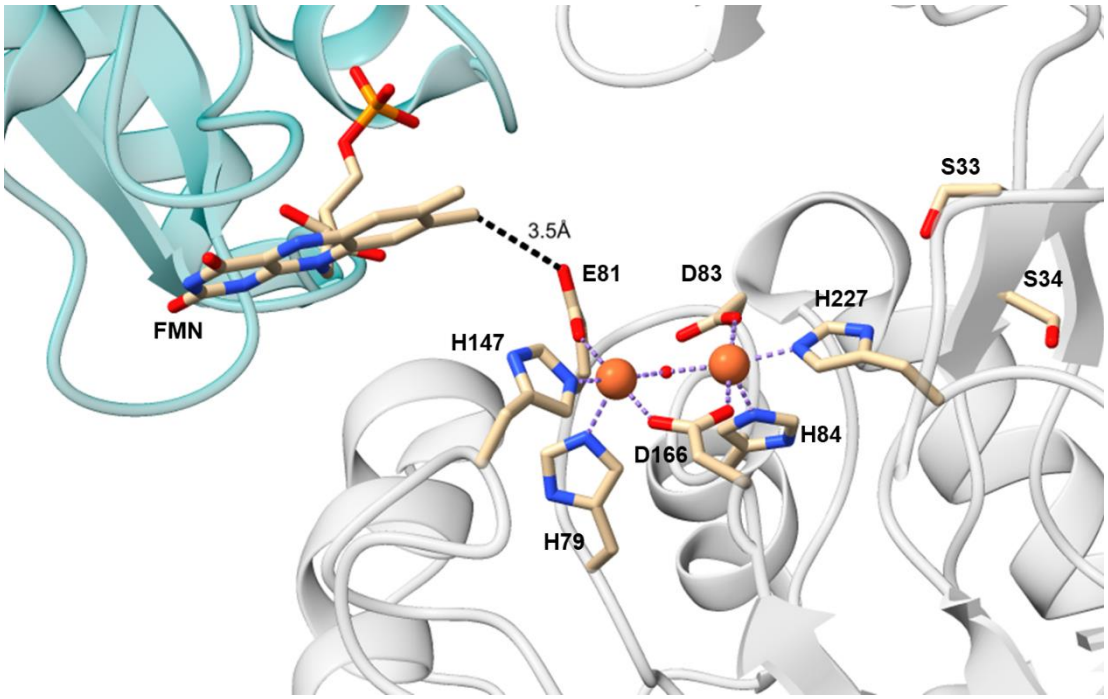

Figure 7 – **Cartoon representation of the interface between two FlRd monomers,** showing the distance between Asp81 and the C8 of the FMN, where electron transfer occurs. The active site and FMN co-factor are represented as sticks. The phosphate molecule present in the original structure, was omitted for better visualisation.

1.5.5. Flavorubredoxins

As mentioned above, *E. coli* flavorubredoxin (FlRd) was first reported in 1998 by Wasserfallen and co-workers [30] and is, currently, one of the most studied FDPs and the only FlRd studied so far. It belongs to Class B and is found in the Proteobacteria phylum, specifically in the beta, delta and gamma classes. [21]

Besides the common flavodiiron core, Class B FDPs contain a C-terminus rubredoxin-like domain that harbours a $FeCys_4$ centre. The rubredoxin domain is linked to the flavodiiron core by a 20 amino acids long flexible coil that in solution is found protruding out of the homotetramer. [43] Rubredoxins are small proteins that participate in redox reactions and that are usually composed of approximately 50 amino acids. They present one iron atom as a cofactor that is coordinated by four sulphur atoms from four cysteines in a tetrahedral geometry. These four cysteines are usually

a part of two sets of the Cys - $X_{(1-4)}$ - Cys - Gly motif, distant in the primary structure by *ca.* 30 residues in the canonical rubredoxins and by about 12 residues in short-chain rubredoxins.[44]
The FlRd from *E. coli* is the only FDP studied until now that presents a clear preference for nitric oxide reduction contrarily to the other FDPs, whose preferred substrate is molecular oxygen or reduce both substrates with similar rates. It is a 54 kDa protein encoded by the *norV* gene, having a total of 479 amino acids, 400 of them being from the flavodiiron core. [23]

FlRd production by *E. coli*, a facultative anaerobic gram-negative bacterium present in the human gut, reveals that this organism possesses a scavenging or an attenuating mechanism to cope with the damage intended by the innate immune system with the NO production as a source of nitrosative stress. Also, the low oxygen reduction activity of this enzyme can be seen as an advantage for the bacterium if using an anaerobic metabolism, since the concentration of oxygen in the human gut can vary up to 60 µM. [22, 45]
Bioinformatics analysis of the amino acid sequences from Class B FDPs revealed the presence of a highly conserved motif - $G_{32}S(T)SYN_{36}$ - present in a loop region near the active site (data not published), that is also quite conserved in the other Classes of FDPs. The presence of conserved serines or threonines in the motif seems to indicate an important role of the hydroxyl functional group in those specific positions. Further bioinformatic analysis were carried out, this time to assess putative phosphorylation sites in flavorubredoxins and resulted in high probabilities for phosphorylation in serines 33 and 34. Since the hydroxyl group in serines and threonine residues are known to be very common phosphorylation site, two putative phosphorylation sites were then hypothesised.

1.6. Post Translational protein modifications – phosphorylation

Phosphorylation, or the addition of a phosphoryl group to the side chain of an amino acid, is one of the most common and important post-translational protein modifications. This modification is known to constitute a main reversible regulatory mechanism controlling cell growth, differentiation and activation or inactivation of important metabolic pathways, amongst others. The addition of a phosphoryl group to an amino acid sidechain leads to major changes in the protein structure, namely by conferring negative charges that can serve as new hydrogen bonds acceptors or by altering the environment due to phosphoryl's large size. These changes can affect protein location inside the cell and its stability, leading to the activation, inhibition, or inactivation of the enzyme, thus creating changes in the metabolic pathways the protein is involved in. Protein phosphorylation is catalysed by kinase enzymes, while the removal of a phosphate group, or dephosphorylation, is catalysed by phosphatase enzymes. [46]

However, the great variety of kinases and phosphatases reported so far makes it a very difficult task to identify which kinases and phosphatases are responsible for specific phosphorylations. To assess the presence of a phosphorylation site in a protein without finding the kinase responsible for it, a few techniques were developed throughout the years. These techniques, summarised by Chen, Z. and co-workers [46] in 2015, can include phosphate mimicking, incorporation of phosphoamino acids into the proteins, total or semi synthesis of proteins and also site-directed mutagenesis (usually the first approach).

In site-directed mutagenesis for phosphorylation assessment, amino acids that are known to be the most common targets for phosphorylation present in the position under study (usually serines, threonines, tyrosines or histidines) are mutated to other specific amino acids, according to the type of amino acid under study and the type of effect desired. In the case of serine and threonine phosphorylation assessment, those amino acids can be replaced by an alanine residue, while the replacement of a serine or threonine by an aspartate or glutamate, respectively, will mimic a phosphoserine or phosphothreonine. After mutating the amino acids the whole characterisation of the protein is done and compared to the wild-type protein to verify what changes the phosphorylation or dephosphorylation would cause in the protein under study. [46]

2. Objective

Flavorubredoxin, or FDP from *E. coli*, is currently one of the most studied flavodiiron proteins. The presence of a conserved motif near the active site (- $G_{32}S(T)SYN_{36}$ -) amongst Class B FDPs raises questions about the role that these amino acids play in the protein's function. Between those conserved amino acids, the presence of two conserved hydroxyl sidechain groups is noticeable (33 and 34, in *E. coli* numbering), from serine and/or threonine residues in different organisms.

In this experimental work, two site-directed mutants (S33D and S34D) were studied to give insights about the role played by serines 33 and 34 in FlRd biochemical features, as well as in FlRd activity towards its substrates (molecular oxygen, hydrogen peroxide and nitric oxide).

Bioinformatic analysis showed high probabilities for phosphorylation in serines 33 and 34 leading to the hypothesis that serines 33 and 34 could be phosphorylation sites. Thus, the substitution of serine residues by aspartates could be used as mimicking of a phosphate bound in positions 33 and 34. The analysis of the kinetical, spectroscopical and structural properties would then give some insights about the role played by serines 33 and 34 in protein activity as well as in the phosphorylation state of the residues.

3. Materials and methods

All the reagents used in this experimental work are highly pure and provided by Merck, Sigma Aldrich, NZY Tech, GE Healthcare or Lab Chem.

3.1. Plasmid isolation – FlRd

The *E. coli norV* (encoding flavorubredoxin) gene synthesis as well as its site-directed mutants and cloning into the expression plasmid, *pET-24a*, were performed by GenScript. The plasmid construction was optimised for *E. coli* codons. Plasmid isolation and replication was obtained upon transformation by heat shock in *E. coli* XL1 Blue and *E. coli* DH5-α competent cells. The transformation process started by incubating the desired cells with 80 ng of each plasmid mentioned above in ice for 30 minutes. Following that, the heat shock was performed in a water bath at 42 ºC for 40 seconds and then the cells were cooled in ice for 2 minutes. After the heat shock process, 900 µL of liquid Lysogeny Broth (LB) medium (composition in appendix 8.1) containing kanamycin (50 µg/mL) were added to each transformation tube and incubated for 1 h 30 min, at 37 ºC, 150 rpm.

After transformation, cells were placed in LB-Agar plates (composition in appendix 8.2) containing kanamycin (50 µg/mL) and incubated overnight at 37 ºC. Subsequently, one colony of each plate was inoculated in 5 mL of LB medium and grown overnight at 37 ºC, 150 rpm. Cells were harvested by centrifugation, at 9400 x*g*, for 10 min and then each plasmid was isolated using the Miniprep kit (NZYTech).

3.2. FlRd production

A pre-inoculum containing a single colony of *E. coli* BL21 (DE3) Gold cells transformed with the desired plasmid (transformation was performed as mentioned in section 3.1), was grown overnight at 37 ºC, 150 rpm in LB medium containing kanamycin (50 µg/mL). Then, 8 L of minimal medium (M9) enriched with 100 µM of iron chloride (composition in appendices 8.3 and 8.4) were inoculated with 3% of the pre-inoculum and allowed to grow until an optical density (OD) of 0.4 was reached. At this point, expression of the desired plasmid was induced with 100 µM of isopropyl β-D-1-thiogalactopyranoside (IPTG) and the media supplemented with 100 µM of iron chloride.

After 6 h of growth, cells were harvested by centrifugation at 9400 x*g*, for 10 min, disrupted in a French Press apparatus at 16000 psi (Thermo) in a three-cycle process and resuspended in 20 mM Tris-HCl, pH 7.5. After that, the soluble extract was separated from the cellular debris and membrane fraction by centrifugation at 18500 x*g* (Beckman Coulter), for 30 min and ultracentrifugation at 140000 x*g*, (Beckman Coulter) for 1h 30 min, respectively.

3.3. FlRd purification

Protein (wild type, S33D and S34D) purification was performed by ion exchange chromatography in a 50 mL Q-Sepharose (GE Healthcare) column previously equilibrated with 20 mM Tris-HCl, pH 7.5, 18% glycerol. Both proteins were eluted with a gradient, from 0% to 50% of 1M NaCl, in 20 mM Tris-HCl, pH 7.5, 18% glycerol, in a total volume of 600 mL; the protein was eluted at approximately 300 mM of NaCl.

Resulting fractions were analysed by SDS-PAGE and UV-Visible spectroscopy and the purest fractions were pooled based on the ratio between their absorbances at 450 nm and 280 nm.

The proteins were concentrated in a Diaflo (Amicon) cell with a membrane with 30 kDa cut-off. In this step, the buffer was exchanged from 20 mM Tris-HCl, pH 7.5, 18% glycerol, 300 mM NaCl to 50 mM Tris-HCl, pH 7.5, 18% glycerol.

3.4. FlRd reductase production

The *E. coli norW* (encoding flavorubredoxin-reductase) gene synthesis and cloning into the expression plasmid, *pET-24a*, was performed by GenScript. The plasmid construction was optimised for *E. coli* codons. The transformation and the pre-inoculum processes were done as described in Sections 3.1 and 3.2. Then, 8 L of LB medium were inoculated with 3% of the pre-inoculum and allowed to grow until an optical density (OD) of 0.6 was reached. At this point, expression of the desired plasmid was induced with 100 µM of IPTG. After 4 h of growth, cells were harvested and lysed as described in Section 3.2.

3.5. FlRd reductase purification

Initially, reductase purification was done as described in Section 3.3 for FlRd, but the resulting fractions were not satisfactorily isolated, requiring another purification step. In the second

purification step, a 20 mL column with an anionic Fractogel resin (Merck) column previously equilibrated with 20 mM Tris-HCl, pH 7.5, 18% glycerol was used, with a gradient of from 0% to 50% of 1 M NaCl, in a total volume of 400 mL; the protein was eluted at approximately 100 mM of NaCl.

Resulting fractions were analysed by UV-Visible spectroscopy and the purest fractions were pooled based on the ratio between their absorbance at 450 nm and 280 nm. The protein was concentrated as described in Section 3.3.

3.6. Iron, flavin and protein quantification

3.6.1. Iron quantification

The amount of iron present in the protein sample was assessed through a colorimetric method. In this assay, the reaction of Fe^{2+} with o-phenanthroline leads to the formation of a reddish complex, with an absorbance maximum at 510 nm. The process can be described by the following reaction:

$$3\ (1{,}10-\text{phenanthroline})\ +\ Fe^{2+} \rightarrow [\text{Fe}-phen_3]^{2+} \qquad \text{Equation 5}$$

Initially, it is necessary to unfold and precipitate the protein allowing for the release of the non-covalently bound cofactors by the addition of hydrochloric acid (HCl) and trichloroacetic acid (TCA). To determine the total amount of iron, it must be in the ferrous (Fe^{2+}) redox state, which can be guaranteed by the addition of a mild reducing agent, such as hydroxylamine chloride used in this experiment for that purpose. [47]

To determine the iron content in the sample, a calibration curve was built, using 8 assay tubes and their duplicates containing increasing amounts of an iron standard solution (0.01 mg/mL).

After that, in duplicate, 100 µL of protein solution and 300 µL of Milli-Q water were added to an Eppendorf tube, followed by the addition of 50 µL of HCl 8 M to each tube. After 15 minutes of incubation at room temperature, 50 µL of TCA was added to each tube and the tubes were incubated for 30 more min at room temperature. The samples were centrifuged for 5 minutes, at 8000 rpm. Posteriorly, each supernatant was divided into two parts of 150 µL. To each Eppendorf tube it was added 400 µL of 10% hydroxylamine chloride and vortexed. Finally, 400 µL of 0.3% (w/v) 1,10-phenanthroline was added to each tube, incubated at room temperature for 2 hours and the absorbances at 510 nm were measured. The determination of the iron content was performed using the equation of the calibration curve.

3.6.2. Flavin quantification

The determination of the flavin present in the protein sample was performed by UV-Vis spectrophotometry, by measuring the absorbance at 450 nm, considering that the extinction coefficient of oxidised FMN is 12,500 M^{-1} cm^{-1}. [48]

The process started by the addition, in duplicate, of 100 µL of protein solution and 300 µL of Milli-Q water to an Eppendorf tube, followed by the addition of 5 µL of HCl 8 M to each tube. After 15 min of incubation at room temperature, 50 µL of TCA was added to each tube and the samples were incubated for 30 more min at room temperature. Subsequently, the samples were centrifuged at 8000 rpm for 5 min and the pellet discarded. Posteriorly, ammonium acetate was added to the solution in order to neutralise the solution, a visible spectrum of the supernatant was performed and the absorbance at 450 nm was used to determine the non-bound flavin concentration.

3.6.3. Protein quantification

Protein quantification was done using the Bradford colorimetric assay. This assay is based on the binding of a dye, Coomassie Blue G-250, to the protein under study. Under acidic conditions, this dye is doubly protonated and is red, while under neutral conditions it is green and under basic conditions, anionic form, it is blue. When in contact with the protein in its cationic form, it will be able to donate one electron to charged groups at the surface of the protein, causing structural alterations and exposure of hydrophobic pockets that will be stabilised by the dye's sulfonic acid groups and also by Van der Waals interactions. After stably bound to the protein, the dye becomes unprotonated and the whole complex protein-dye becomes blue.

The red form of the dye presents an absorbance maximum at 470 nm while the blue form of the dye presents an absorbance maximum at 595 nm. Since the amount of blue anionic complex is directly proportional to the amount of protein in solution, it is possible to determine the amount of protein present in that solution by measuring the absorbance at 595 nm. [49]

A calibration curve was built using bovine serum albumin (BSA) as standard protein (0.5 mg/mL) and the determination of the protein concentration was done using the calibration curve that was built between 0 and 7.5 mg of standard protein.

3.7. Protein quaternary structure determination

The quaternary structure determination of the recombinant proteins was assessed by size exclusion chromatography using a 25 mL Superdex S-200 10/300 GL column (GE Healthcare), previously equilibrated with 20 mM Tris-HCl, 150 mM NaCl, pH 7.5, 18% glycerol. The calibration curve was performed using thyroglobulin (669 kDa), apoferritin (443 kDa), β-amilase (200 kDa), alcohol dehydrogenase (150 kDa), bovine serum albumin (66 kDa) and carbonic anhydrase (29 kDa) as standard proteins. Blue dextran was used as void volume marker (2000 kDa).

With the elution volumes and the logarithm of the molecular masses of the standard proteins, a calibration curve was built and the molecular mass of the proteins under study could be determined.

3.8. SDS-PAGE

Protein production and purification efficacy were assessed by sodium dodecyl sulphate-polyacrylamide gel electrophoresis (SDS-PAGE), 12.5% and 15% of acrylamide. All the SDS-PAGE done were in the presence of β-mercaptoethanol, a reducing agent used to break disulphide bonds between cysteine residues, allowing for a complete denaturation of the protein.

Samples were prepared by the addition of sample buffer up to a total volume of 15 µL and heated for 10 min. Low Molecular Weight (LMW) Protein Marker II (NZYTech) was used as molecular mass marker.

After polymerisation, the gels were placed in an electrophoretic chamber (BioRad) and immersed in running buffer. After loading the samples in their corresponding wells, gels were run at 80 V, 40 mA for 15 min, then at 180 V, 40 mA for 1 more hour. The composition of the buffers used in the SDS-PAGE technique is presented in appendix 8.5.

3.9. Agarose gel

The quality of the isolated plasmids was assessed by an agarose gel 0.8% (w/v). The gel was prepared by dissolving 0.64 g of agarose powder in 80 mL of tris-acetate-EDTA (TAE) buffer (40 mM Tris, 20 mM acetate, 1 mM EDTA, pH 8.6), followed by heating of the mixture until complete dissolution. After that, 2 µL of NZYTech Sybr dye was added and the solution was

placed in the electrophoretic chamber (VWR Avantor) to polymerise. After polymerisation, the gel was immersed in TAE buffer.

Samples were prepared by the addition of NZYDNA loading dye to make up a total volume of 10 µL, loaded in their corresponding well and the gels were run at 80 V, for 1 h 30 min. The molecular mass marker used was NZYTech Ladder III. The composition of the buffer used in the agarose gel technique is presented in appendix 8.6.

3.10. Stability assays

Circular dichroism (CD) is a spectroscopic technique that uses the chirality of certain molecules, such as proteins, to measure the differential absorption of polarized light. The result of this interaction is an elliptical polarized light that is used to determine specific parameters such as the content of alpha-helices, beta-sheets and loops present in the secondary structure or, with the variation of the temperature, the variation of the secondary structure and the melting temperature. Ellipticity is the unit of circular dichroism and the thermodynamics of protein unfolding can be studied by monitoring the variation of the ellipticity at a certain wavelength as a function of temperature. [50]

CD thermal assays of flavorubredoxin wild type and mutants were performed using a JASCO J-850 CD spectrometer connected to a Peltier temperature controller. Each solution containing the protein in 20 mM Tris HCl pH 7.5 was adjusted to a final concentration of 0.2 mg/mL. CD measurements were carried out in a cuvette with a 0.1-cm path length.

Thermal denaturation studies were carried out by heating each sample from 5 °C to 90 °C in steps of 5 °C, and the ellipticities were measured using the same parameter settings described above. At each temperature, the sample was equilibrated for 2 minutes prior to the CD measurements.

The maximum molar ellipticity values at 225 nm were normalized and fitted to the Boltzmann sigmoidal curve (Equation 6) using Origin 2019 software where dx is the slope of the curve. Y is the molar ellipticity value, x is the temperature, and T_m is the melting temperature. [51]

$$Y = y_{min} + \frac{y_{max} + y_{min}}{1 + e^{(T_m - x/dx)}} \qquad \text{Equation 6}$$

3.11. Oxygen reduction assays

Oxygen reduction assays were performed amperometrically in a Clark-type oxygen electrode, in an Oxygraph 2K (Oroboros Instruments). The Oxygraph 2K apparatus is composed by two cylindrical glass chambers placed in a temperature-controlled copper block and equipped with oxygen sensors. The chambers are closed with a conical titanium stopper sealed with Viton O-rings, preventing exchanges with the exterior environment when completely closed. Inside the chamber, polyetheretherketone (PEEK) stirrers can be placed to guarantee the homogenisation of the solutions.

The O2k measures the amount of O_2 dissolved in an aqueous solution at 2 second intervals. The signal of each chamber is converted and transmitted to a software (DatLab) where the graphics of the variation of the oxygen concentration as a function of time are displayed, allowing for real-time monitoring of the oxygen concentration inside the chambers.

The consumption of oxygen by the electrode can also be measured, decreasing linearly with the decrease of oxygen partial pressure. Besides that, the oxygen diffusion in the chambers must also be taken into consideration, increasing linearly with the pressure difference between the external environment and the medium inside the chambers. Thus, the total rate of oxygen consumption or generation is the slope observed for each experiment corrected for the contribution of the electrode consumption and the background oxygen diffusion. [52]
All the oxygen assays were performed in 50 mM Tris-HCl, pH 7.5, 18% glycerol, with 5 mM NADH, 0.7 µM FlRd-reductase, 1 µM FlRd mutants and 64 nM catalase as final concentrations. All the experiments were performed at 25 ºC.

At the beginning of the assays, buffer, NADH and catalase were added to the assays, the chambers were partially closed and the oxygen concentration was allowed to stabilize. O_2 concentrations were varied between 260 µM and 10 µM by the addition of argon. Then, chambers were completely closed and, after a short time of oxygen consumption by the electrodes, FlRd-reductase was added, followed by the addition of FlRd (S33D, S34D or wild type) after 45 seconds. The reaction was allowed to proceed until an oxygen concentration of approximately 1 µM and, at this point, 3 µL of a saturated solution of sodium dithionite was added to ensure a full reduction of the oxygen present.

Data were calibrated in DatLab, relatively to the maximum and minimum amount of oxygen, then exported to a datasheet and evaluated in Excel. Data were represented in graphics showing the oxygen concentration as a function of time. The data processing consisted in determining the slopes of the experimental curve right before and after the addition of the protein under study. Protein activity was obtained by subtracting the slope corresponding to the oxygen consumption

by the FlRd-reductase from the slope corresponding to all constituents in solution. The determination of the kinetic parameters was done with GraphPad Prism 8.4.3 software.

3.12. Hydrogen peroxide reduction assays

Evaluation of the hydrogen peroxide reduction activity was performed under anaerobic conditions, in an anaerobic chamber (Coy Lab Products). Protein activity was assessed by monitoring NADH concentration in the cuvette by UV-Vis spectrophotometry (Shimadzu UV-1603 spectrophotometer) at 340 nm, which is the maximum of the absorption band for reduced NADH. [51]

Assays were performed in 50 mM Tris-HCl, pH 7.5, 18% glycerol, with constant concentrations of NADH (200 µM), reductase (0.7 µM), protein (2 µM) and variable concentrations of hydrogen peroxide (from 5 µM to 400 µM).

The determination of the H_2O_2 concentration was also performed by UV-Vis spectroscopy. Experiments were initiated by running a spectrum from 200 to 500 nm for two H_2O_2 dilutions (100 µL:1100 µL and 200 µL:1200 µL), using the extinction coefficients 72.8 $M^{-1}.cm^{-1}$ at 230 nm and 43.6 $M^{-1}.\ cm^{-1}$ at 240 nm. [53,54] H_2O_2 concentration was determined for each new solution prepared.

H_2O_2 reduction assays were started by setting the software (UVProbe 2.33) in the kinetics mode, with an assay time length of 150 seconds and monitoring the NADH consumption through the decrease of the absorbance at 340 nm, ($\varepsilon_{340\ nm}$ = 6.22 $mM^{-1}.\ cm^{-1}$). [55] Initially, buffer and NADH were added to a cuvette, leading to an initial absorbance of approximately 1.0 at 340 nm. Then, the assay was started in the software, with constant magnetic agitation, followed by rapid addition of FlRd-reductase, proteins under study and H_2O_2, the last one in variable final concentrations, and the assay was carried out for 150 seconds. The order of addition of the protein and H_2O_2 was alternated amongst the assays.

Subsequently, the datasheets were exported and the data were treated with Excel. To determine the rate of H_2O_2 reduction by the protein, the assays were represented in graphics as absorbance at 340 nm as a function of time. The slope after the last addition in each experiment, determined by linear regression, was considered the activity of the protein at that concentration of hydrogen peroxide. The determination of the kinetic parameters was done with a non-linear fit adjusted by the Solver Excel tool by minimising the sum of the squares of the differences between the experimental data and the theoretical data calculated with a given value of K_M and V_{max},

optimising these values, and with GraphPad Prism 8.4.3 software to confirm the analysis with Excel tool and to determine the error of the fitted curves.

3.13. Nitric oxide reduction assays

NO reduction rates by the FlRd mutants were determined using Apollo 4000 (World Precision Instruments). In this system, NO molecules diffuse through the selective electrode membrane and are oxidized at the working electrode, generating an electric current that is proportional to the amount of NO present in solution, and can be converted to concentration. These assays were based on the addition of a known amount of NO and on the posterior monitoring of the rate of NO concentration decrease when the FlRd mutants were added into the system. [56]

The preparation of the NO saturated solution was done by the addition of gaseous NO to a sealed flask containing buffer 50 mM Tris-HCl, pH 7.5, 18% glycerol, that was kept in ice during the procedure.

All the samples were degassed and 10 mM of glucose and 375 nM of glucose oxidase were added to reduce the oxygen present in the chamber prior to the addition of the other components. 750 nM of catalase was also added to consume the hydrogen peroxide generated by the reaction catalysed by glucose oxidase.

After approximately 10 minutes of equilibration, three successive additions of 2 µL of a saturated NO solution were performed resulting in a final NO concentration of approximately 12 µM. Posteriorly, NADH (5 mM), FlRd reductase (0.7 µM) and the protein under study, wild type or mutants (200 nM), were added, in that order, making up a total volume of 1000 µL.

It was then possible to observe the process of NO consumption by the FlRd proteins, as the data were displayed in the software Apollo 4000, version 4.1.4 (World Precision Instruments) as an electrical current as a function of time.

Data were then exported as datasheets and evaluated in Excel. To process these data, it was necessary to convert the current produced at the electrode to NO concentration. That was done by relating the amount of current produced when a certain concentration of NO was added in the successive additions mentioned above. Subsequently, the slope of the curve right after the addition of the FlRd protein was determined as the initial velocity.

3.14. X-ray crystallography

X-ray crystallography is a widely used technique that allows for three-dimensional structure determination of proteins and other biomolecules. The experimental procedure consists of

crystallization of a highly purified sample under specific, known and optimised conditions, such as temperature, pH, purity, the concentration of protein and precipitant, precipitant agent, buffer, amongst others. There are a few crystallisation methods, the most used being vapour diffusion, through hanging or sitting drop. This process is based on a phase transition mechanism, where the protein transits from a liquid and unorganised state, present in an unsaturated solution, to a highly organised state (crystal structure), in a supersaturated solution of the precipitant agent, resulting in nucleation followed by growth of the protein crystals. [57]

The crystals are, then, exposed to an X-ray beam resulting in a diffraction pattern that gives part of the information needed to determine the structure. The other part of the information can be calculated by several techniques, such as Molecular Replacement (MR), Single/Multiple Anomalous Dispersion (SAD/MAD) or Single/Multiple Isomorphous Replacement (SIR/MIR). Thus, a first density map can be calculated and the model further refined in an iterative process. The objective of this process is to improve the agreement between the modelled structure and the reflections obtained in the experimental diffraction pattern to fit the density map more accurately. To verify the quality of the refinement several parameters must be analysed, for instance, the relationship between R-work and R-free and the Ramachandran outliers, amongst others. [58]

The substitution of a conserved amino acid by another can lead to various consequences, one of them being a protein structural change that can go from mild to very severe. A crystallographic study was carried out to assess the impact of the substitution of Ser33 and Ser34 by an aspartate in the FlRd structure.

3.14.1. Initial screening process

The experimental procedure started by screening for the best crystallization conditions for the mutant proteins under study. Two crystallization screenings, the Basic Chemical Space (BCS) and the Structure Screen 1+2 HT-96, both commercialised by Molecular Dimensions, were chosen to begin with. The screening process was done in a 96 well plate, by the sitting drop method and prepared using a Mosquito LCP crystallography robot.

3.14.2. Scale-up

For S33D, two conditions from the BCS screening were chosen to be scaled-up, while for S34D only one condition was chosen. For S33D the chosen conditions were B9 (0.1 M Tris-HCl, pH 8.5, 20% PEG Smear High) and E11 (0.05 M magnesium chloride, 0.05 M sodium citrate, 0.1 M Bis-Tris propane, pH 7.8, 22.5% PEG Smear High); and for S34D the chosen condition was A5 (0.1 M phosphate citrate, pH 5.5, 25% PEG Smear Medium).

The scale-up process was performed in a 24 well plate and each condition was scaled-up with three proportions of protein to precipitant agent: 1:1, 2:1 and 1:2, and done in duplicate. In total, six wells for each condition. The hanging drop crystallization method was used in this process.

3.14.3. Screening at different temperatures and with additives

After the scale-up process, it was necessary to try new approaches at different temperatures and with the presence of additives. For that, three BCS screening plates (96 wells), identical to the first BCS screening, were prepared for S33D and incubated at 4 ºC, room temperature and 35 ºC.

A fourth 96 well plate was used to optimize the condition E11 of BCS screening, mentioned above. In this optimization, performed at the Mosquito LCP crystallography robot, all the reservoirs of the plate were filled with the E11 solution and to each well a different additive (Morpheus Additive Screen, Molecular Dimensions) was added to assess if and which additive would stimulate the growth of robust crystals. Three proportions of protein to precipitant (1:1, 1:2 and 2:1) were tested in each well.

Another screen was performed for S34D, this time with "Structure 1+2" screen, in the presence of FlRd wild type seeds in order to create nucleation sites and induce crystal growth.

3.15. Electron Paramagnetic Resonance

Electron Paramagnetic Resonance (EPR) is a spectroscopic technique that detects species that have unpaired electrons. This technique is widely used due to its ability to identify paramagnetic species, such as free radicals and many transition metals, that play an important role in vital processes.

Electrons are known to possess a "spin" that confers a magnetic property called magnetic moment. When in the presence of a magnetic field, two distinct energy levels are originated, according to the alignment of the magnetic momentum with the magnetic field. Initially, the lower energy level (parallel) is more populated than the level with higher energy. When the electrons are irradiated with a microwave frequency with an energy equal to the energy gap between the two energy levels created by the external magnetic field, i.e. in a resonance condition, the lower energy electrons are excited and transit to the upper energy level (antiparallel).

To achieve the resonance condition, the microwave frequency is fixed and a sweeping of magnetic field is done. That way, the resonance condition is obtained at the specific field value at which the electron absorbs the microwave radiation.

Since the EPR is the only technique that unambiguously identifies paramagnetic systems, this technique is often used in the study of metalloproteins to understand their electronic properties and structure. [59]

Both protein mutants' samples were prepared in an anaerobic glove box (Coy Lab Products) to a final concentration of 200 μM and were partially reduced upon incubation with 100 μM menadiol. All the samples' spectra were recorded with a Bruker EMX spectrometer, equipped with an Oxford Instruments ESR-900 continuous flow helium cryostat.

4. Results

4.1. Biochemical characterisation

Protein production was successfully achieved for both S33D and S34D mutants in *E. coli* BL21 (DE3) Gold. Protein production was assessed by 12.5% SDS-PAGE, after cell lysis and before the purification step, shown in Figure 8.

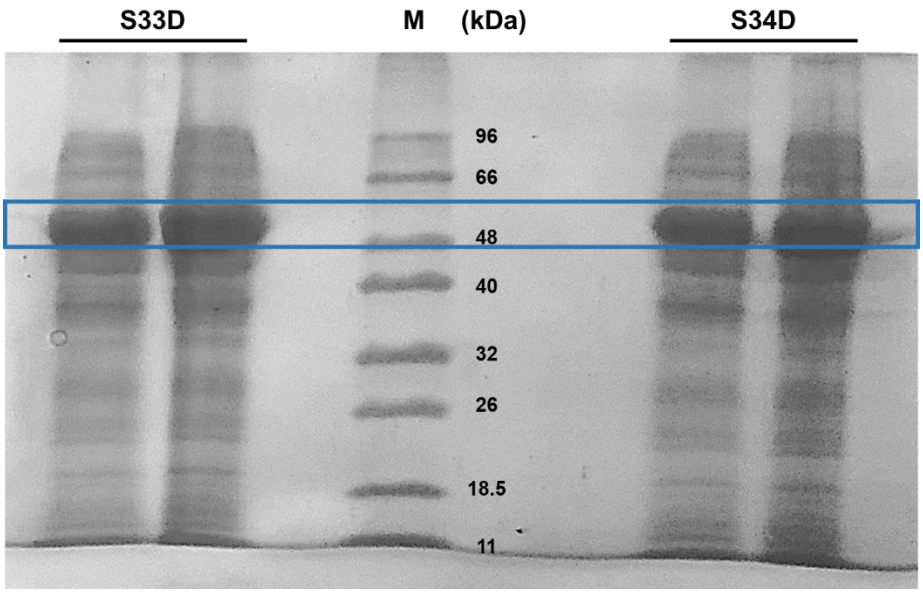

Figure 8 – **SDS-PAGE (12.5%) analysis of protein mutants' overproduction in *E. coli* BL21(DE3) Gold**. **S33D** - first and second lane correspond to a load of 2 and 4 uL of the same sample, respectively; **M** - Molecular mass marker; **S34D** - first and second lane correspond to a load of 2 and 4 uL of the same sample, respectively.

By analysing the SDS-PAGE gel it is possible to observe a great variety of bands corresponding to the proteins naturally produced by the bacteria. Since each monomer of the proteins under study has a molecular mass of 54 kDa, a large band was expected in each well between the bands correspondent to 66 and 48 kDa of the molecular mass marker, which is observed in the gel. That way, the match of the expected electrophoretic migration pattern with the ones actually observed indicates that the proteins of interest were successfully produced. Additionally, the contrast observed between the intensity of the bands of interest with the other bands present in the same lane indicate that the gene that encodes for the protein of interest was effectively overexpressed when induced with IPTG.

Protein elution in the Q-Sepharose column was achieved at 300 mM of NaCl. After protein purification, the purity of the resulting fractions was assessed by SDS-PAGE (Figure 9) and the iron and flavin contents were determined, as well as the protein concentration. The ratios of iron to protein and flavin to protein were also calculated and are shown in Table 1.

By analysing the gels, it was possible to observe that the mutants' purification was successful due to the almost complete absence of other bands besides the one corresponding to the proteins of interest.

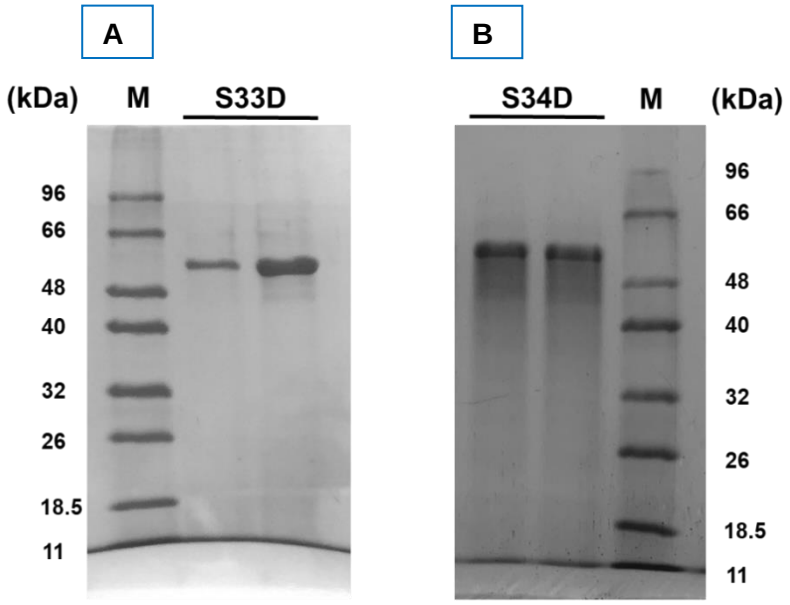

Figure 9 – **SDS-PAGE** (12.5% and 15%, for panels A and B, respectively) **analysis of the purity of the fractions after the purification step**. **S33D** - first and second lane correspond to a load of 0.5 and 1 µL of the same sample, respectively; **M** - Molecular mass marker; **S34D** - first and second lane correspond to a load of 1 and 0.5 µL of the same sample, respectively.

Table 1 – **Evaluation of flavin and iron incorporation in FlRd overproduction**, measured through iron and flavin to protein ratios.

	S33D	S34D
[Iron] / [Protein]	2.17 ± 0.06	2.13 ± 0.11
[Flavin] / [Protein]	0.66 ± 0.01	0.57 ± 0.04

The growth of S33D and S34D mutants resulted in 1.97 and 2.43 g of cells/L and 55.2 and 54.2 mg of pure protein/L, respectively. Iron quantification revealed that the total incorporation in the proteins was of approximately two iron atoms per monomer, for both mutants. The expected value would be three iron atoms, two from the diiron site and one from the rubredoxin domain. However, when comparing to previous reported studies [30, 60, 62], this partial incorporation of iron is common in similar proteins overproduced in *E. coli*.

Flavin quantification showed that full flavin incorporation was not obtained as well: each monomer should have one flavin cofactor present in the flavodoxin-like domain. Since the FMN is non-covalently bound to the protein, the whole process from cell lysis until protein concentration may lead to the loss of the cofactor. Besides that, protein exposure to light, even

transiently, can cause flavin photoreduction and degradation. Nevertheless, the same extent of FMN content is within the range observed for other FDPs overproduced in *E. coli*. [39,62]

The UV-Visible spectra obtained for both mutants (Figure 10, Panel A), present typical flavin and rubredoxin features characterised by peaks with maxima at 378 and 478 nm, characteristic of flavins, and a broader band at 570 nm, resulting from the rubredoxin site. The spectra obtained for the mutants are similar to each other and also to the ones of the wild type FlRd (Figure 10, Panel B). [30]

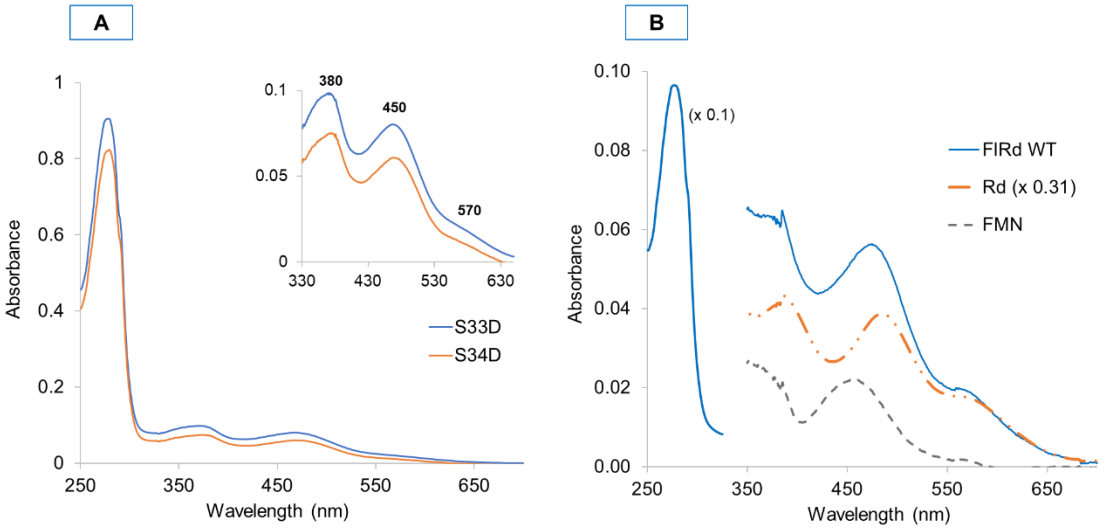

Figure 10 – **UV-Visible spectra of wild type FlRd and protein mutants, S33D and S34D, as purified**. **Panel A**- S33D and S34D full spectra, blue and orange, respectively. The inset represents a 10x zoom of the spectra, between 330 and 630 nm. **Panel B** – Wild type FlRd spectrum. The blue full line represents the FlRd wild type spectrum, while the orange dashed dot and grey dashed lines represent the rubredoxin domain spectrum (x 0.31) and the FMN domain spectrum, the last one resulting from the subtraction of the rubredoxin spectrum from the FlRd wild type spectrum.

The quaternary structure determination by gel filtration revealed that both proteins were present in solution as a tetramer, as the wild type enzyme described by Wasserfallen and co-workers.[30] The chromatogram of the gel filtration for both mutants, corrected for the void volume molecular marker, is represented in Appendix 8.7. All the previous reports indicate that the minimal functional quaternary structure is a dimer, indicating that FlRd mutants studied in this experimental work fulfil the minimal condition for a functional protein. [62]

4.2. Stability studies

To assess whether the mutations would affect protein stability, the melting temperatures were determined by measuring CD spectra at increasing temperatures (Figure 11). The determined T_ms 55 ºC and 59 ºC, for the S33D and S34D mutants, respectively, were very similar to that of the wild type enzyme (54ºC), indicating that no significant changes in the protein stability were induced by the mutations, besides a slight stabilisation that could be due to the establishment of new interactions.

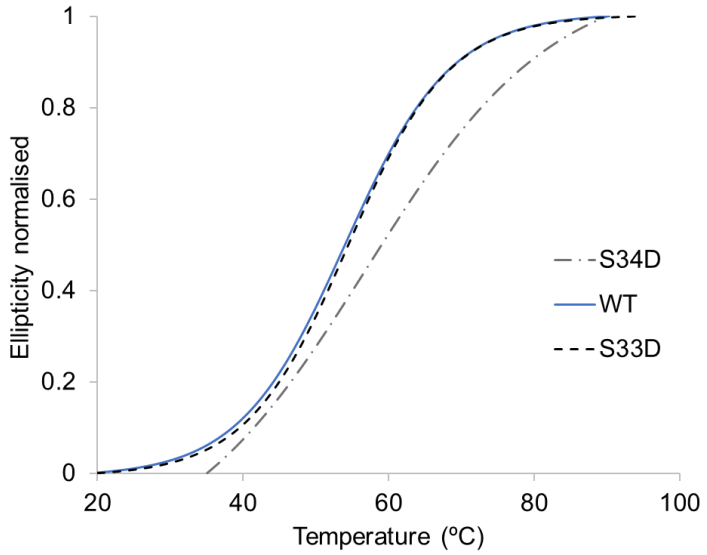

Figure 11 – **Circular dichroism analysis of the melting temperature for the wild type FlRd and its mutants (S33D and S34D).** Variation of the ellipticity normalised as a function of the temperature for the wild type protein (blue full line), S33D (black dashed line) and S34D (grey dashed dot line).

4.3. Kinetic characterisation

To determine the influence of a phosphorylation in the putative phosphorylation site under study, kinetic assays for the three known FlRd substrates were carried out. In these assays the comparison between the kinetic parameters obtained for the wild-type protein and for the mutants could give some insights on the effect of the mutations under study in the enzyme.

4.3.1. Oxygen reduction assays

The study of oxygen reduction by the wild type protein in the presence of a large initial concentration of NADH, catalase and under saturating concentrations of oxygen (equivalent to the oxygen naturally dissolved in a buffer solution under atmospheric pressure, approximately 260 μM), can be represented by the graphic shown in Figure 12.

In these assays, it was possible to observe that when 0.7 μM FlRd-reductase was added to the chambers, prior to FlRd wild type addition, the amount of oxygen inside the chamber started to decrease at a low rate of approximately $0.14 \pm 0.02\ s^{-1}$. The reductase reduces oxygen to hydrogen peroxide, and it is for this reason that catalase is added in the assays. When 1 μM of the protein wild type was finally added, a faster reduction of oxygen occurs, with a turnover rate of $1.61 \pm 0.26\ s^{-1}$.

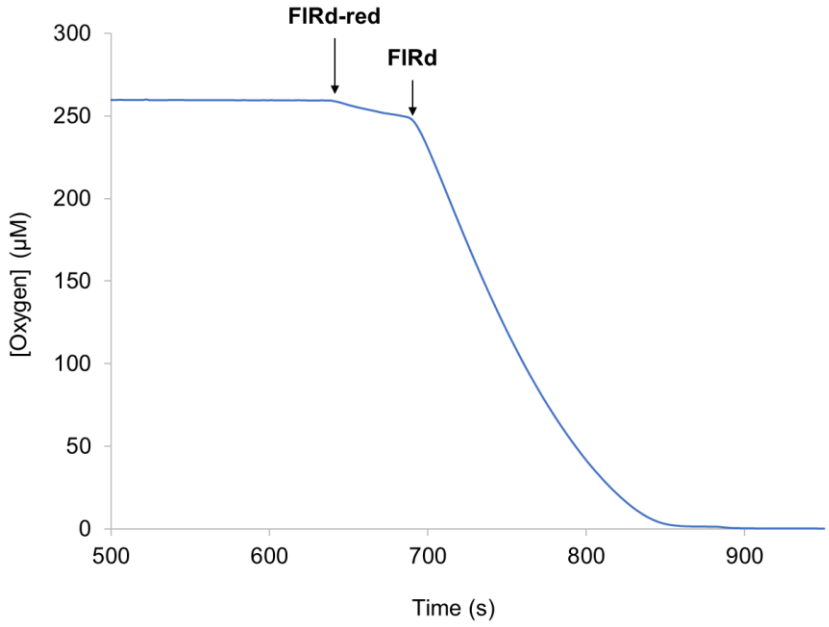

Figure 12 – **Typical graphical representation of oxygen reduction assays with FlRd wild type and mutants, performed in Oxygraph 2K**. **FlRd-red -** correspond to the addition of FlRd-reductase to the assay; **FlRd -** correspond to the addition of FlRd or mutants to the assay.

The oxygen reduction by the mutants S33D and S34D, under the same conditions used for the assays with the wild type protein, yielded turnover values of 1.93 ± 0.37 s^{-1} and 1.89 ± 0.32 s^{-1}, for S33D and S34D, respectively. These rates were slightly higher than the one determined for the wild type protein but were within the experimental error determined.

In order to determine the type of kinetics followed by this protein and its mutants, a set of experiments with variable concentrations of oxygen were carried out, resulting in a set of initial velocities data, similar to the one represented in Figure 12 but having as starting point several different oxygen concentrations. The summary of all experiments and their fitted curves assuming a Michaelis-Menten behaviour (Figure 13) resulted in V_{max} values of 1.75 ± 0.19, 2.62 ± 0.19 and 2.47 ± 0.17 µM/s, while the K_M values were 19.8 ± 11.5, 25.4 ± 8.6 and 30.2 ± 10.5 µM, for wild type, S33D and S34D, respectively.

It was possible to observe a small increase in the V_{max} of oxygen reduction when Ser33 and Ser34 were mutated to aspartates comparatively to the wild type protein; however, a small increase was also observed for the K_M of the reaction with the mutant FlRds, indicating a slight decrease in the affinity of the protein for the oxygen molecule. It should be mentioned that, due to experimental limitations, it was not possible to perform the assays at lower oxygen concentrations, and so the K_M values may be overestimated.

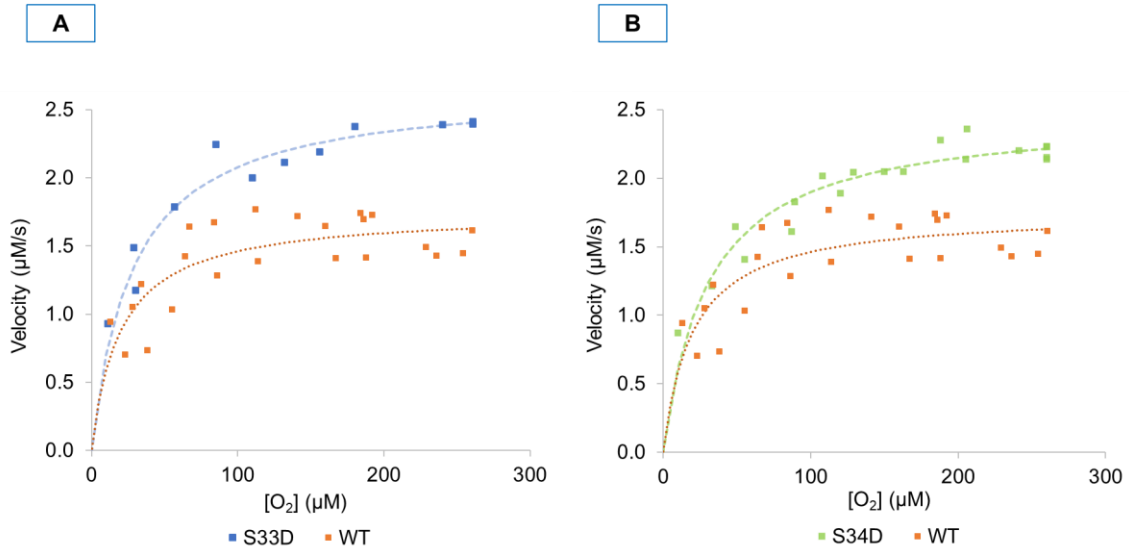

Figure 13 – **Michaelis Menten analysis for the oxygen reduction activity.** Kinetic analysis performed using the GraphPad software. **Panel A** - Comparison between S33D (blue dashed line) and FlRd wild type (orange dotted line); **Panel B** - Comparison between S34D (green dashed line) and FlRd wild type (orange dotted line).

The small difference in the results obtained for the mutants when compared to the wild type protein, are probably associated to the high variability verified in the wild type dataset, and observable in the graphics shown in Figure 13. Due to the methodology used it was not possible to have multiple experiments with the same initial oxygen concentration and therefore, to calculate an error associated to each assay. However, the error associated to the fit of the curve and, consequently, the error associated with the determination of the kinetic parameters was calculated with GraphPad software and resulted in the standard deviation for each parameter.

4.3.2. Hydrogen peroxide reduction assays

The study of hydrogen peroxide reduction by the FlRd protein and its mutants under anaerobic conditions was performed by measuring spectrophotometrically the consumption of NADH (at 340 nm) as a function time, at a certain concentration of hydrogen peroxide (Figure 14).

In these experiments it was observed that the addition of FlRd-reductase to a solution with NADH did not cause any variation in NADH concentration. The posterior addition of FlRd caused a small consumption of NADH, enough to reduce all the FlRd present in solution through the FlRd-reductase.

The subsequent addition of H_2O_2 led to a faster decrease of the NADH present in solution, showing that the FlRd protein in fact has the ability of reducing H_2O_2 having NADH as primary electron donor. In order to exclude the possibility of the NADH consumption being due to H_2O_2 reduction by the FlRd-reductase, the order of addition of FlRd and H_2O_2 was alternated and it was observed that the fast NADH consumption would only happen when both, H_2O_2 and FlRd, were present in solution.

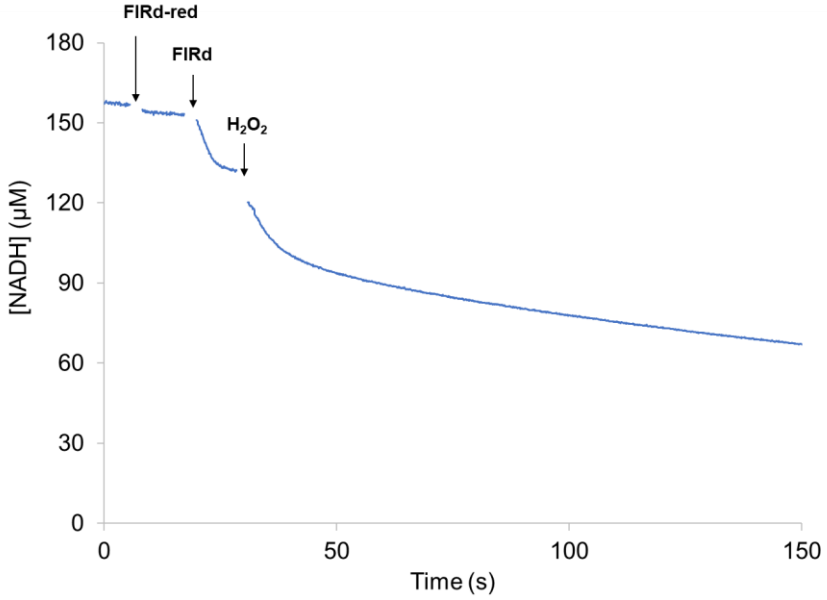

Figure 14 – **Typical graphic representation of hydrogen peroxide reduction assays with FlRd wild type and mutants, performed under anaerobic conditions**. **FlRd-red -** corresponds to the addition of FlRd-reductase to the assay; **FlRd** – corresponds to the addition of FlRd or mutants to the assay; **H_2O_2** – corresponds to the addition of hydrogen peroxide to the assay.

Several assays with different concentrations of H_2O_2 were carried out in order to determine the type of kinetics followed by this protein and its mutants when reducing hydrogen peroxide to water. The data were plotted against each H_2O_2 concentration and a hyperbolic-like curve was obtained, suggesting, once again, a Michaelis-Menten kinetics. Data were, then, fitted to a Michaelis-Menten curve and kinetic parameters could be determined.

The kinetic parameters' determination resulted in K_M values of 42.72 ± 2.66, 18.67 ± 2.52 and 18.44 ± 2.0 µM, and in V_{max} values of 4.92 ± 0.11, 3.73 ± 0.10 and 4.93 ± 0.13 µM/s, for wild type, S33D, S34D, respectively (Figure 15). Comparatively to the wild type protein, the substitution of Ser33 by an aspartate seem to lead to a small decrease of the maximum velocity and a small increase of protein affinity to hydrogen peroxide. The substitution of Ser34 by an aspartate does not seem to alter the maximum velocity, but also causes a slight increase in the affinity for the substrate.

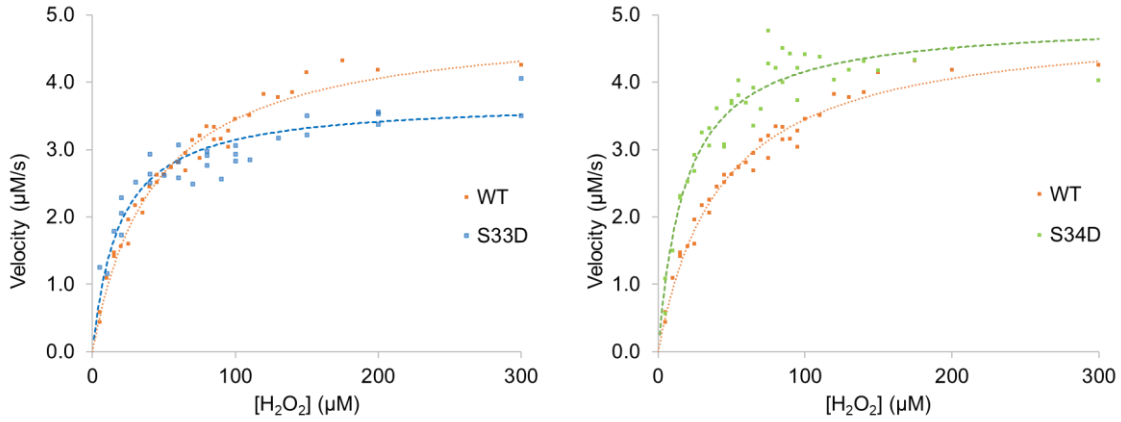

Figure 15 – **Michaelis Menten analysis for the hydrogen peroxide reduction activity.** Kinetic analysis performed in Solver tool in Excel and GraphPad software. **Panel A** - comparison between S33D (blue dashed line) and FlRd wild type (orange dotted line); **Panel B** - Comparison between S34D (green dashed line) and FlRd wild type (orange dotted line).

No reported studies on the FlRd activity towards hydrogen peroxide were previously performed. Such an activity was thus far only described for a class F FDP from *C. difficile 630*, that presents a hydrogen peroxide reductase activity with a turnover of approximately 2 s^{-1} at 100 μM of H_2O_2,[26] while the turnovers determined in this experimental work, at the same concentration of H_2O_2, were 1.76 ± 0.04 s^{-1}, 1.56 ± 0.12 s^{-1} and 1.75 ± 0.31 s^{-1}, for the wild type, S33D and S34D proteins respectively. However, by analysing the curves shown in Figure 15 and looking at the values of K_M determined in this experimental work, it was possible to observe that, at 100 μM of H_2O_2, the condition of saturating substrate was not fulfilled and the activity observed was not a part of the plateau of the curve yet, indicating that the turnover observed for the wild type protein and its mutants at that concentration do not correspond to the maximum velocity.

4.3.3. Nitric oxide reduction assays

NO reduction assays were also performed in order to evaluate the activity of the wild type protein and its mutants, S33D and S34D (Figure 16).

In these assays, the addition of FlRd-reductase does not cause any decrease in NO concentration, indicating that this protein does not have NO as substrate, whereas the addition of FlRd, in the presence of FlRd-reductase, leads to a large and fast decrease in NO concentration.

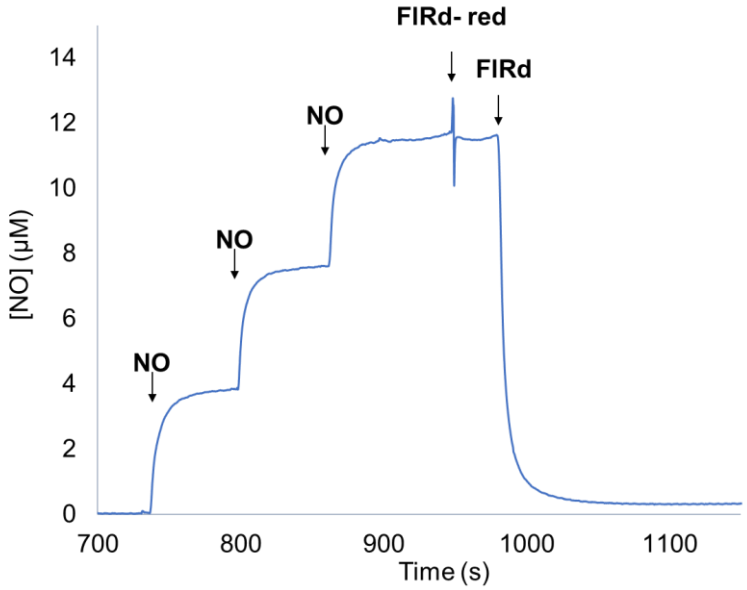

Figure 16 – **Typical graphic representation of nitric oxide reduction assays with FlRd wild type and mutants, performed under anaerobic conditions**. **NO** - addition of nitric oxide to the assay; **FlRd-red** - addition of FlRd-reductase to the assay; **FlRd** - addition of FlRd or mutants to the assay.

The calculated turnover of NO reduction under saturating concentrations of NADH (5 mM) with a final concentration of NO of approximately 12 µM for the wild type protein was 11. 1 ± 1.1 s^{-1}. This turnover is very similar to the one reported by Gomes and co-workers of 14.9 ± 6.7 s^{-1}, [23] under the same conditions. However, the substitution of Ser33 and Ser34 by an aspartate led to the decrease of the NO reduction rate to 5.4 ± 0.5 s^{-1} and 6.0 ± 0.4 s^{-1}, respectively.

It was not possible to determine the kinetic parameters for NO consumption due to technical constraints.

4.4. Structural characterisation

4.4.1. X-ray Crystallography

In order to find the best crystallization condition, thermofluor assays were carried out to determine the stability of the protein and its mutants in different buffers. A set of 96 buffers (composition in Appendix 8.8) was tested for protein stability and it was determined that buffer 100 mM Tris-HCl, pH 7.4, 250 mM NaCl was the most appropriate for the two mutants.

- **S33D**

S33D crystals started to be observed after 2 weeks of incubation at room temperature in 10 conditions of the BCS screening plate, three of them shown in Figure 17. Crystals from conditions A5, A11, B5, B6, B8, B9, C6, E7, E11 and H7 were sent to a synchrotron facility and analysed, however no diffraction pattern could be obtained.

Conditions B9 (0.1 M Tris-HCl, pH 8.5, 20% PEG Smear High) and E11 (0.05 M $MgCl_2$, 0.05 M sodium citrate, 0.1 M bis-tris propane, pH 7.8, 22,5% PEG Smear High) were scaled-up and, after four weeks, wells correspondent to condition E11 presented robust plaque crystals as shown in Figure 18. Thus, a screening of this condition with additives was performed in order to improve crystallization conditions.

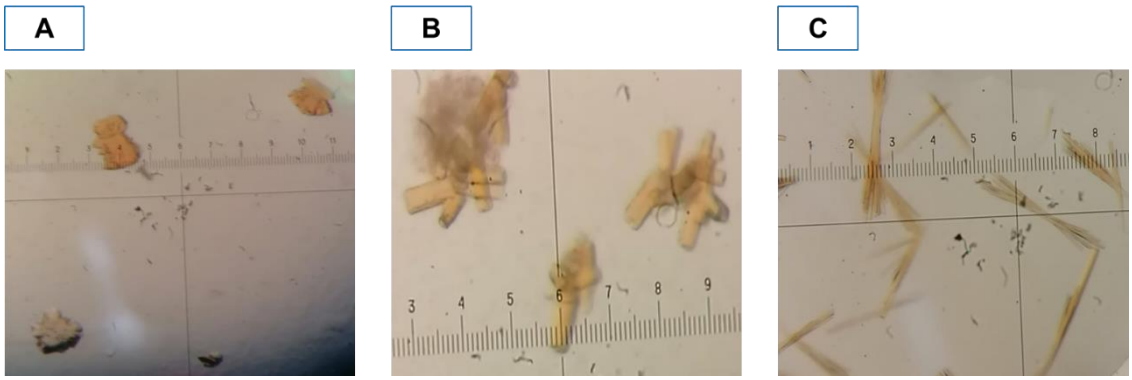

Figure 17 – S33D crystals obtained with the initial BCS screening, at room temperature. **Panel A** - Well B6 (0.1 M bicine, pH 9.3, 25% v/v PEG Smear Medium); **Panel B** - Well B9 (0.1 M bicine, pH 9.3, 25% v/v PEG Smear High); **Panel C** - Well H7 (0.15 M lithium sulphate, 0.05 M magnesium chloride, 0.1 M HEPES, pH7.8, 20% v/v PEG Smear High).

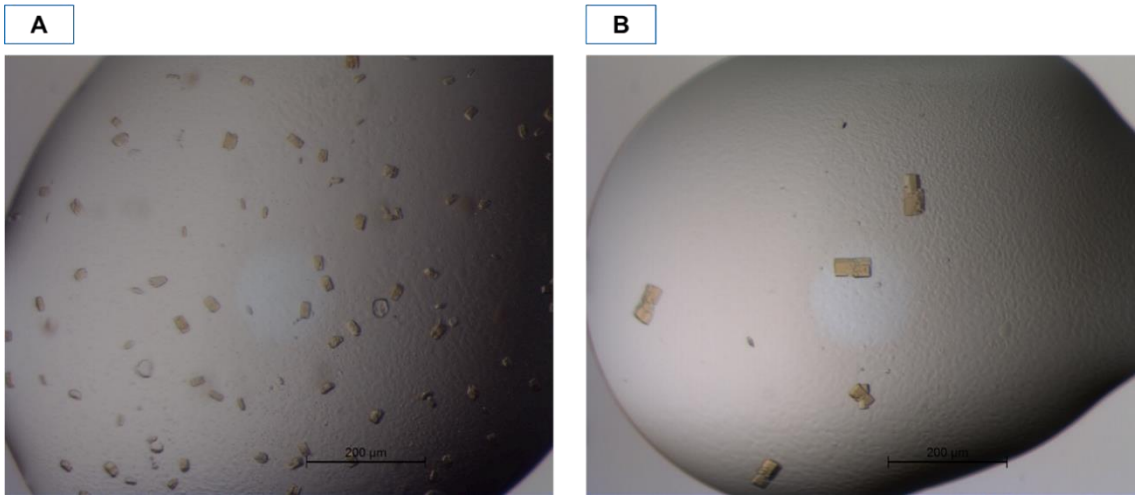

Figure 18 – **S33D crystals obtained after scale-up of condition E11 from BCS screening**. **Panel A** - Well A1 (0.05 M $MgCl_2$, 0.05 M sodium citrate, 0.1 M bis-tris propane, pH 7.8, 22,5% PEG Smear High; 1 protein : 1 precipitant agent); **Panel B** - Well A5 (0.05 M $MgCl_2$, 0.05 M sodium citrate, 0.1 M bis-tris propane, pH 7.8, 22,5% PEG Smear High; 1 protein: 2 precipitant agent).

After a screening with additives having solution E11 as precipitant, plaque-shaped crystals were present in four conditions, shown in Figure 19.

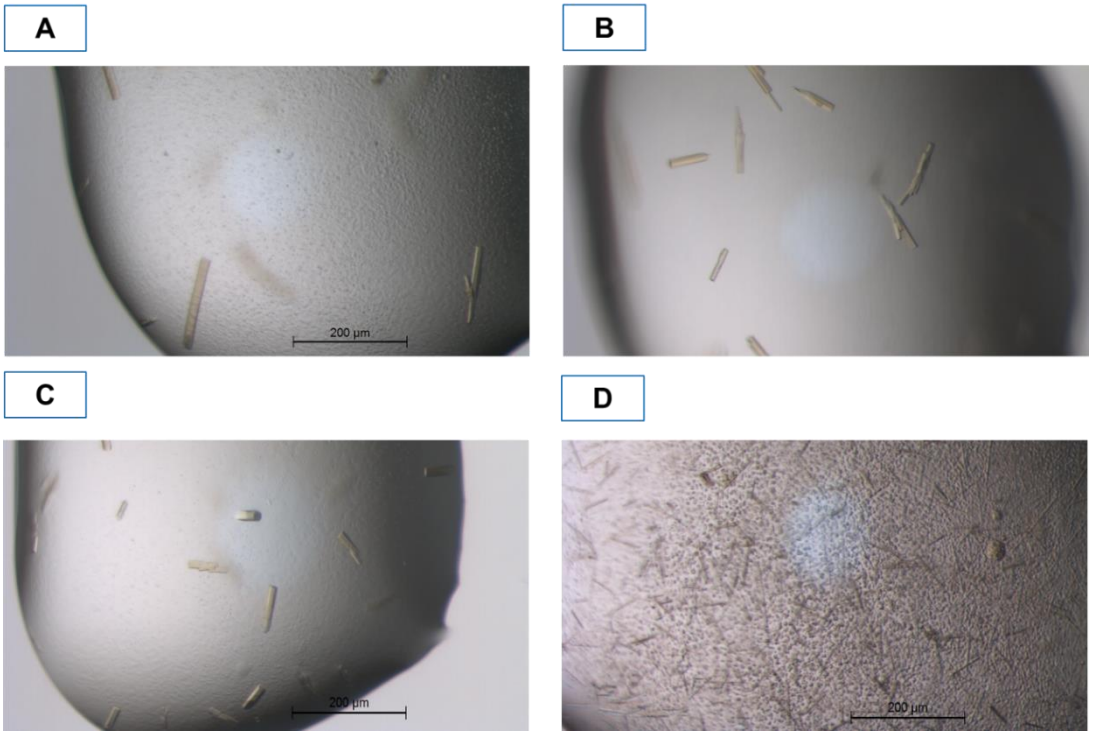

Figure 19 – **Crystals obtained after the screening with additives having condition E11 from BCS screening as precipitant agent** (0.05 M $MgCl_2$, 0.05 M sodium citrate, 0.1 M bis-tris propane, pH 7.8, 22,5% PEG Smear High). **Panel A** - Well A5 (additive: ethylene glycol); **Panel B** - Well C8 (additive: triethylene glycol); **Panel C** - Well E6 (additive: 1,2,6 – hexanediol); **Panel D** - Well E7 (additive: 1,5 pentanediol).

- **S34D**

S34D needle crystals were observed in well A5 (0.1M phosphate citrate, pH5.5, 25% PEG Smear Medium) of BCS screening (Figure 20) and sent to a synchrotron facility.

Even though a few crystallization conditions were found, no diffraction pattern was observed upon exposure to synchrotron radiation, which prevented the determination of the crystallographic structure of FlRd mutants.

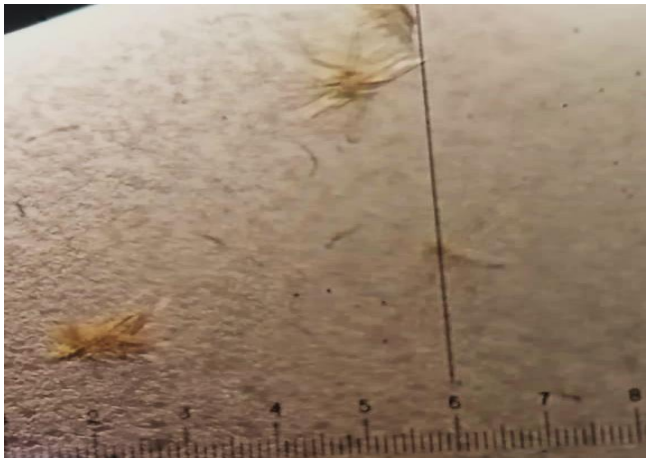

Figure 20 – **Needle crystals observed for S34D in BCS screening**. Well A5 (0.1M phosphate citrate, pH 5.5, 25% PEG Smear Medium).

4.4.2. Electron Paramagnetic Resonance

EPR has been a useful technique to study metalloproteins like the FDPs. With this technique, it was possible to study the rubredoxin domain, as well as the diiron site present in *E. coli* FlRd as described by Gomes, Vicente and co-workers. [60,61]

EPR spectra of FlRd wild type and S33D and S34D mutants as isolated revealed, as expected, an intense rhombic (quasi-axial) signal with three resonances at g~9.17, 4.66 and 4.30, corresponding to the rubredoxin domain. This centre is typically in a high spin configuration with S=5/2 when oxidised, showing an intense EPR signal. Analysing the g values obtained with a rhombogram it was possible to determine that the rubredoxin iron centre possesses E/D values of ~0.2 and ~0.3, corresponding to Kramers' doublets in populational states $|\pm1/2>$ (g_{max}=9.17) and $|\pm3/2>$ (g_{med}= 4.66 and g_{min}=4.30) (Figure 21).

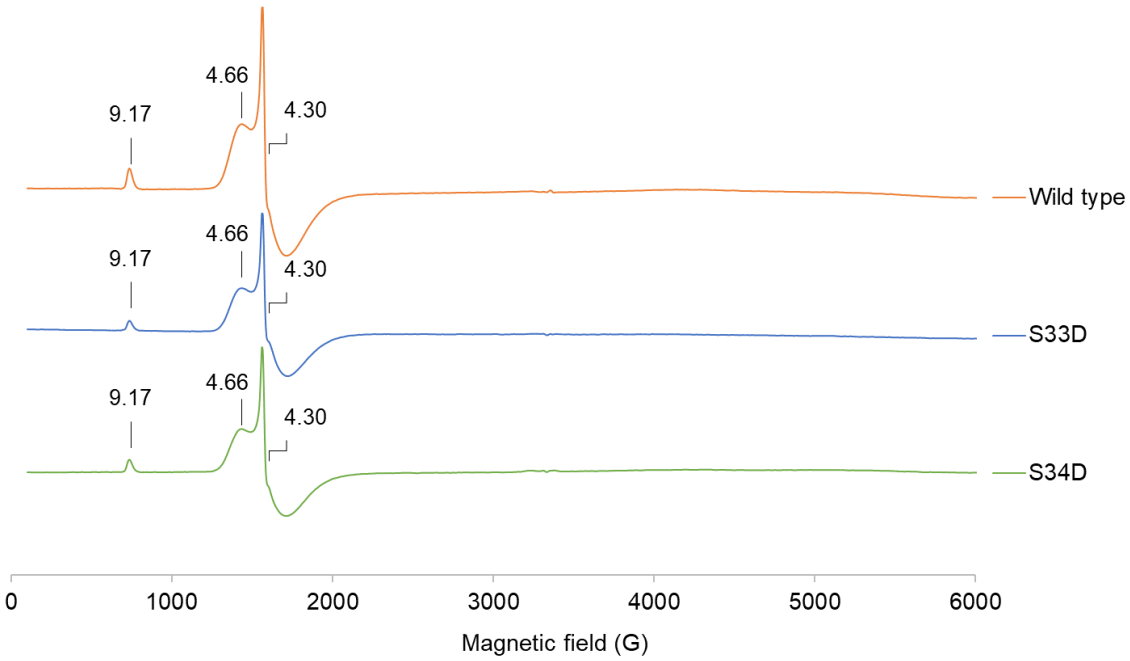

Figure 21 – EPR spectra of the as isolated wild type FlRd (orange) **and mutants, S33D** (blue) **and S34D** (green), **at 7 K**, showing the rubredoxin signal. In the spectra, the rubredoxin g values are represented for each protein. Microwave power: 2 mW; Microwave frequency: 9.41 GHz; Amplitude modulation: 10 G; protein concentration: 200 µM.

It was also worth noting that, in the oxidised state, it was not possible to observe any EPR signal for the diiron catalytic centre as it is antiferromagnetically coupled (S=0) and, consequently, EPR silent. Thus, to obtain a half-integer system spin it was necessary to partially reduce it with 1 equivalent of menadiol. The graphic representation of the EPR spectra of the diiron centre in the oxidised and partially reduced states (with a mixed valence S=1/2, Fe^{III} – Fe^{II}), when it is EPR active, is shown in Figure 22.

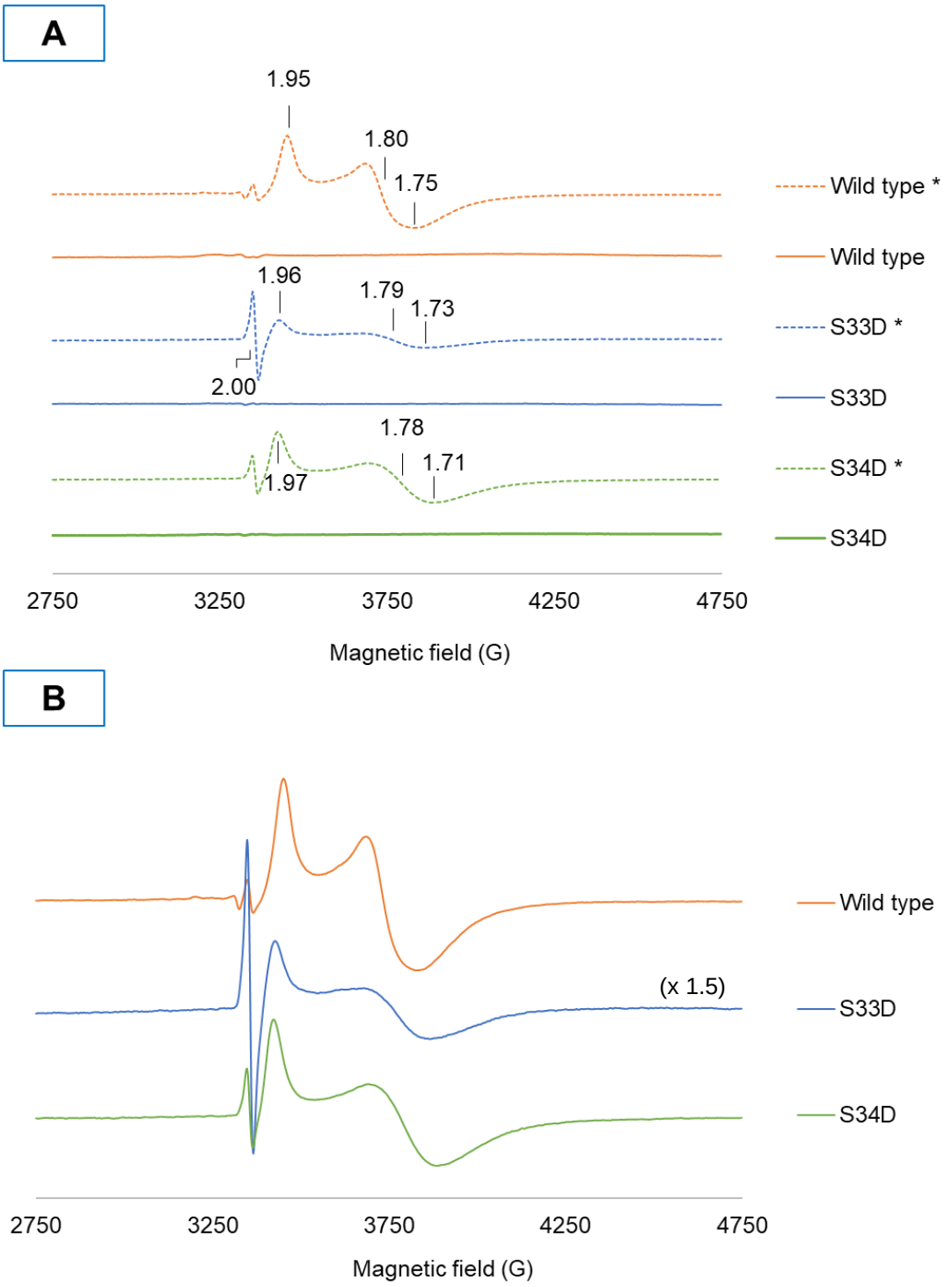

Figure 22 – **EPR spectra of both, oxidised and partially reduced** (*), **FlRd wild type** (orange) **and respective mutants, S33D** (blue) **and S34D** (green), **at 7 K**, showing the signal of the diiron centre and semiquinone radical. **Panel A** – Comparison between the spectra in the oxidised and partially reduced state. Partially reduced proteins' spectra are shown in dotted lines, while oxidised proteins' spectra are shown in full lines. In the spectra, the g values of the diiron centre are represented for each protein and the g value of the semiquinone is represented in S33D partially reduced spectrum. **Panel B** – direct comparison of the partially reduced spectra of FlRd wild type (orange), and mutants, S33D (blue, x 1.5) and S34D (green). Microwave power: 2 mW; Microwave frequency: 9.41 GHz; Amplitude modulation: 10 G; protein concentration: 200 µM.

The EPR spectra obtained for the diiron centre with a mixed valence showed a rhombic (quasi-axial) signal with features around g=1.95, 1.80 and 1.75 for the wild type protein, g=1.96, 1.79 and 1.73 for S33D and g=1.97, 1.78 and 1.71 for S34D. The g-values of the three proteins are very similar, indicating that the diiron centres have essentially identical structures in them. It was also noticeable the presence of an isotropic signal with a g value around 2 attributable to a radical species, most likely correspondent to the semiquinone form of the FMN co-factor.

5. Discussion

The biochemical characterisation of the wild type protein and its mutants indicated that the general properties of FlRd were kept unaltered when Ser33 and Ser34 were mutated to aspartates, namely, iron and flavin content, quaternary structure, and UV-Vis spectra. EPR spectra were also similar to the ones previously reported by Vicente [61] showing the rubredoxin and the diiron catalytic centre with similar parameters and characteristic features.

On the other hand, the comparison between the kinetic results obtained for the mutants and the wild type protein, implicated the premise of a phosphorylated state in the wild type protein. It was not known whether the wild type protein under study was naturally phosphorylated or not in Ser33 and Ser34, and if the interaction with the phosphate group, in case of existing, would be labile or not. However, after several steps of handling without phosphatase inhibitors, including purification and dialysis, steps usually related to cofactor loss, it would be improbable to keep a molecule as a phosphate bound to the protein. Also, even though the crystallographic structure of wild type FlRd shows a phosphate molecule near the active site, the calculated distance between the hydroxyl group of Ser33 and Ser34 and the closest oxygen molecule of the phosphate is 7.6 and 11.6 Å, respectively, what would make a phosphorylation impossible. Mass spectrometry analysis were also carried out (by another lab member) for FlRd wild type and it was found that Ser33 and Ser34 were not phosphorylated according to the mass obtained for residues 33 and 34, corresponding to simple amino acids with no other groups bound.

The analysis of the kinetic data obtained for the mutants S33D and S34D showed no significant alterations in protein's activity towards molecular oxygen and hydrogen peroxide. Based on the evidences of a non-phosphorylated wild type FlRd, these results seemed to indicate that the conservation of Ser33 and Ser34 in the motif under study was not related to a phosphorylation site, since it was expected that mimicking a phosphate bound in that position would have caused a large variation between the mutants and the non-phosphorylated wild type protein. The localisation of Ser33 and Ser34 in the tertiary and quaternary structure of the protein (in an inner beta sheet near the active site) was another evidence of how challenging it would be to phosphorylate them, even as a monomer before dimerization, due to the small accessibility to large molecules such as kinases.

It would be also questionable whether the substitution of the serines by aspartates could be considered a reliable mimicking of a phosphorylation. Even though in a first approach, the presence of a mono negative charge mediating electrostatic interactions, that could be similar to the ones putatively established by a phosphate group, would be enough to give insights about the phosphorylation state of the protein, it should not be discounted that the presence of one negative

charge could not be enough to mimic two negative charges observed in the dianionic molecule of phosphate. In addition, the planar geometry of the carboxylate could also not be the correct one to mimic the tetrahedral geometry of a phosphate molecule, depending on the type and orientation of interactions. A better approach to protein phosphorylation mimicking would be to create a small environment with two negative charges by substituting two subjacent amino acids by aspartates and/or glutamates to achieve the double negative charge added by a putative phosphate molecule [63] or to try other strategies such as the ones described by Chen and Cole [46], summarised in Section 1.6 of the present work.

Since the evidence seem to indicate that the conserved serines are not a phosphorylation site, other hypothesis were explored. The presence of this conserved motif near the active site is not a reason for it to be directly related to catalysis. Instead, it can also be related to the stability of the structure composing the microenvironment around the active site or related to solvent, substrate or product channels. In this case, as the protein activity towards two of the three substrates is kept almost unaltered, it would be unlikely that the mutations would have significantly altered the interactions stablished directly with the active site or the active site itself. Alternatively, the substitution of a hydroxyl group from Ser33 and Ser34 by a carboxylate group from the aspartate sidechain would lead to disruption and/or alteration of putative hydrogen bonds, in case of existing. An analysis with Chimera X software [64], considering the protein as a rigid body and without minimisation of the energy of the model, showed putative hydrogen bonds established by an aspartate in positions 33 and 34. According to the model created, the new hydrogen bonds established by Asp33 would be with Ser34, Tyr35, His171, and His227, whereas the ones established by Asp34 would be with Asp16, Ser33, Cys173 and Gly228, as represented in Figure 23.

In addition, the difference of charges between serines' and aspartates' sidechains could cause the change in electrostatic interactions, stabilizing or destabilizing the surrounding structure. The presence of a more voluminous amino acid could also block, partially or totally, the accessibility of solvent and substrates channels, limiting or preventing the access to the active site. On the other hand, it could also block, partially or totally, the exit channels for the product of the reaction preventing or slowing down the subsequent molecules of substrate from reaching the catalytic site. This last hypothesis seems to fit the observable results and it could explain why NO reduction is the most affected process when Ser33 and Ser34 were mutated to aspartates. The clashes between the mutant aspartates and the surrounding amino acids are represented in Figure 24.

FlRd being an NO reductase, it was expectable that the turnover rates observed for NO reduction were higher than the ones observable for oxygen and hydrogen peroxide reduction, which was confirmed by the kinetic assays shown in Section 4.4.

In case there was a partial blocking of the product's escape route, it is likely that the most affected process would be the one with higher turnover rates (*ca.* 10 times higher to NO reduction) due to the greater need of quickly removing the product from the active site.

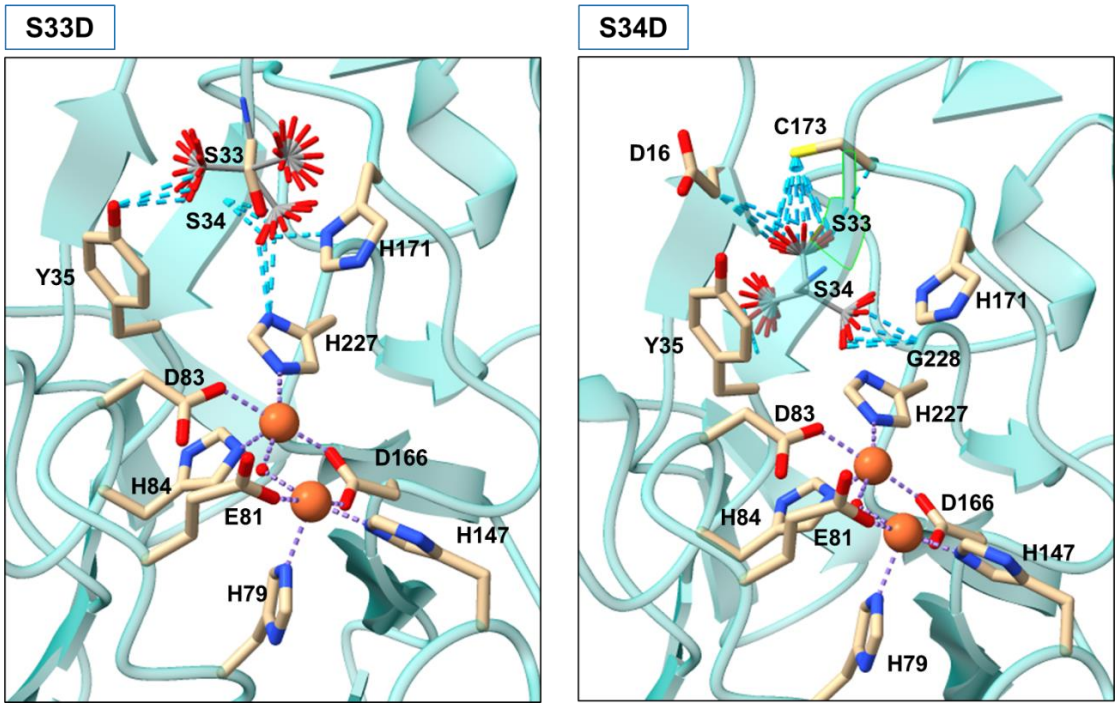

Figure 23 – **Chimera analysis of the putative hydrogen bonds**, represented by the light blue dashed bonds, **established by the aspartate residue (rotamers) if present in positions 33 and 34 of FlRd from *E.coli***. The phosphate molecule coordinating the diiron site present in the PDB structure as well as the secondary structure cartoon representation from positions 18 to 27 were omitted for better visualisation. Panels S33D and S34D refer to the substitution of Ser33 and Ser34 to an aspartate residue, respectively, and the correspondent hydrogen bonds' analysis with aspartate rotamers in each position. The criteria used for this analysis were the ChimeraX default ones: 0.075Å of radius, 0.4 Å of distance tolerance and 20º of angle tolerance.

The study of oxygen and nitric oxide pathways in FlRd from *E. coli* by Romão and co-workers shows the presence of two channels – a longer one with *ca.* 19 Å and a shorter one with *ca.* 8 Å angstroms – that were associated to substrate entrance and product exit route, respectively, according to the density of oxygen and NO molecules observed in each channel, just like described by Victor and co-workers for the rubredoxin:oxygen oxidoreductase (ROO) from *D. gigas* [24]. With Chimera software and, once again, considering the protein as a rigid body and without minimisation of the energy of the protein, it was possible to analyse the proximity between the residues that are part of the channels to Ser33 and Ser34, and infer about the change caused by their substitution by an aspartate residue. The shorter channel described in the study of the structure of FlRd from *E. coli* by Romão and co-workers [40], considered a product escape route, was found to be limited by different amino acids when compared to the amino acids presented by Victor and co-workers [24].

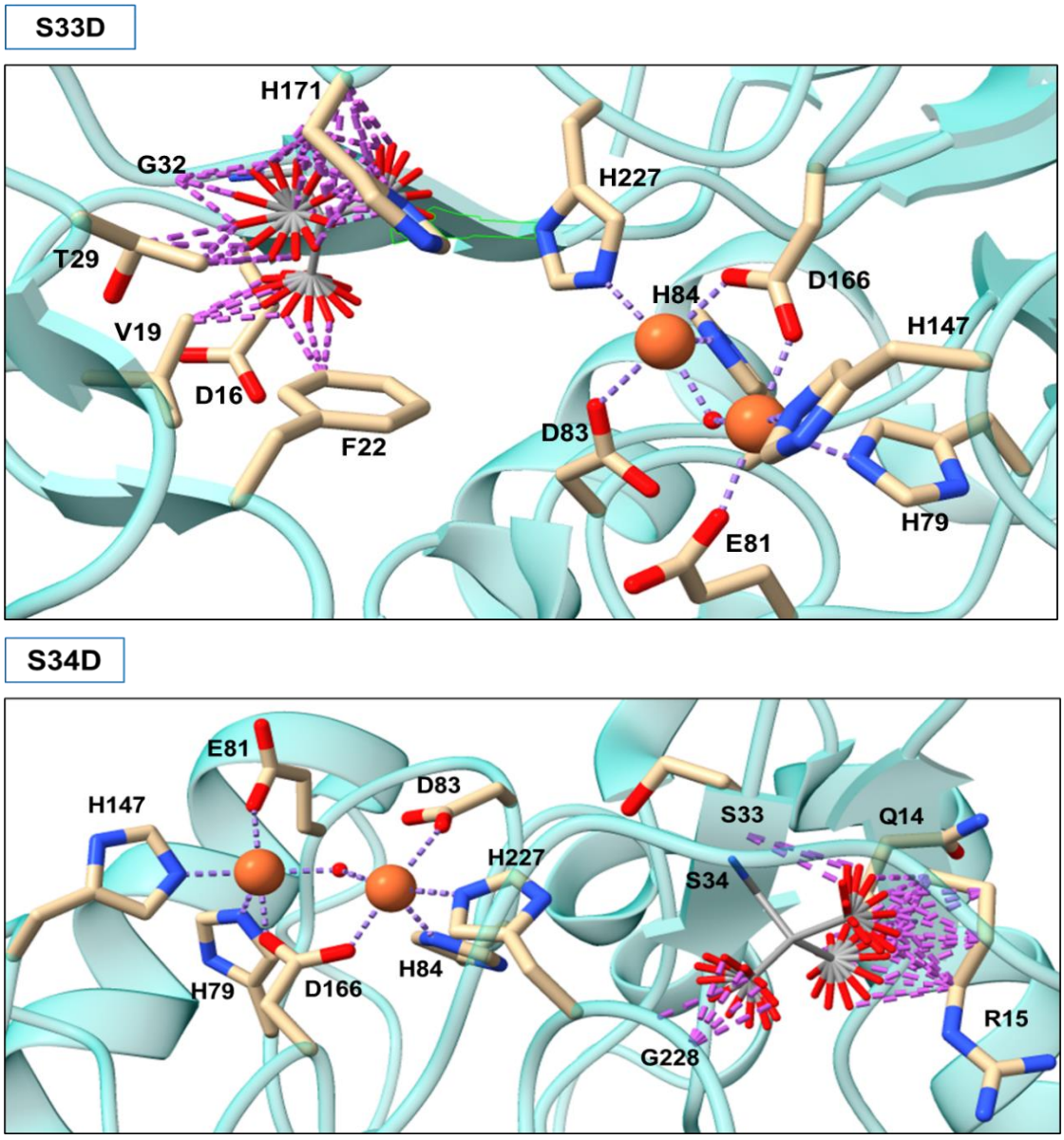

Figure 24 – **Chimera analysis of the putative clashes between amino acids**, represented by the purple dashed bonds, **established by the aspartate residue (rotamers) if present in positions 33 and 34 of FlRd from *E.coli***. The phosphate molecule coordinating the diiron site present in the PDB structure was omitted for better visualisation. Panels S33D and S34D refer to the substitution of Ser33 and Ser34 to an aspartate residue, respectively, and the correspondent clashes analysis with aspartate rotamers in each position. The criteria used for this analysis were the ChimeraX default ones: find residues with Van Der Waals overlap greater than 0.6 Å and subtract 0.4 Å from potential hydrogen bonds.

The FlRd tunnel would start near the active site, going through Val19, Asp21, Tyr35, Asp52, His53, Lys54, Glu82, His113 and Trp148, being the rest of the channel a part of the other monomer and purposely not mentioned here. However, it should be mentioned that, according to Victor and co-workers, the product escape route in ROO starts in Phe23, an amino acid that is also present in FlRd from *E.coli* as Phe22 and is only 4.3 Å apart from Ser33 and from Val19 (Figure 25).

For both channels, from FDPs from *D. gigas* and *E.coli*, the entrance to the tunnel seems to be near Thr/Ser33 and Phe23(*D.gigas*)/22 (*E.coli*), being the distance from Thr33 to Phe23 *ca.* 3.5 Å in ROO from *D. gigas* and the distance between Ser33 and Phe22 *ca.* 4.3 Å in FlRd from *E. coli*. Such a small distance between Ser33 under study and a Phe22 would be a reason for alterations in the microenvironment and partial block of the entrance of the tunnel of the product escape route. A partial block, as discussed above, could be a reason for the decrease of reduction activity and be the limiting step of the reaction of NO reduction, but not in oxygen and hydrogen peroxide that present slower turnover rates.

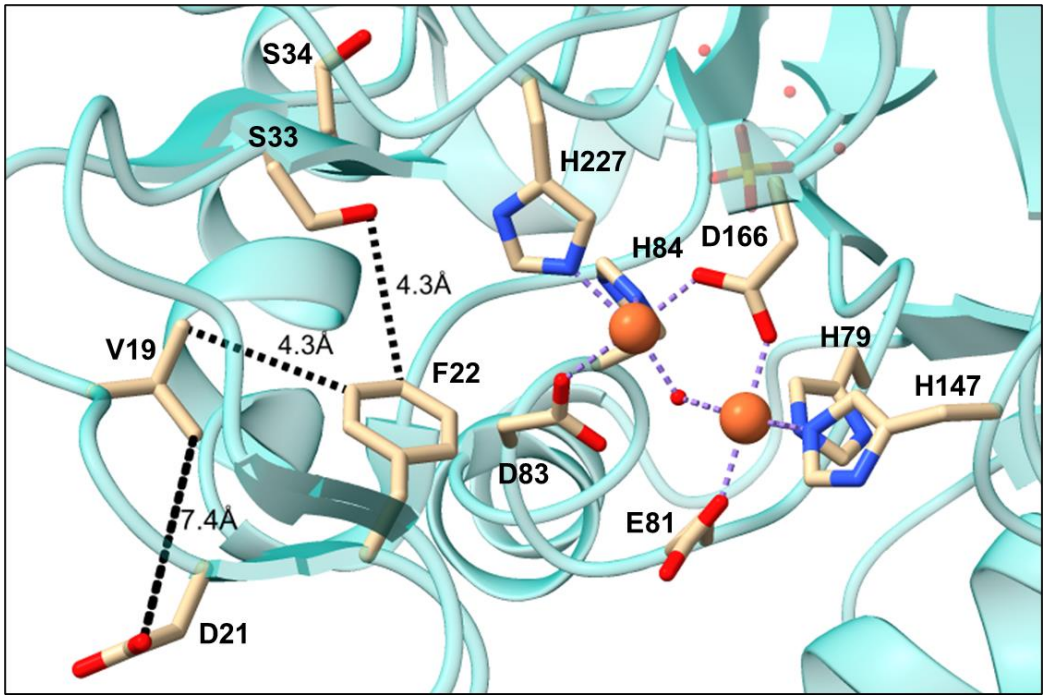

Figure 25 – **Chimera analysis of the distances between Ser33 and Phe22.** It is also shown the distance between the first two amino acids of the product escape channel (V19 and D21) in FlRd from *E.coli.*

The analysis of the possible orientations of an aspartate residue substituting Ser33, performed in the Chimera software, with the structure obtained for the FlRd from *E. coli* (PDB code: 4D02), without any energy minimisation, showed 18 possible orientations, but not equally probable. The most probable orientation (32% of probability) presents four stereochemical constraints, with residues Phe22, Val19, Asp16 and Ser 34. The clash possibility with residues Phe22 and Val19 seems to indicate that the hypothesis concerning the blocking of the product escape route described above could be valid in the case of S33D mutation. The other 17 possible orientations present probabilities of 16% or less of happening and include stereochemical constraints with the residues Phe22, Asp16, Val19, Ser34, Gly32, His171 and Thr29. Besides that it was also observed that, from the 18 orientations analysed, 8 also present the possibility of establishment of hydrogen bonds with residues Tyr35, Ser34, His171 and His227.

The same analysis was carried out with Chimera for the S34D mutant. In this analysis 19 possibilities were found for aspartate rotamers substituting Ser34, but once again, not equally probable. The most likely orientation has a probability of 21% although presenting 5 stereochemical constraints with residues Arg15 and Gln14. The other 18 positions present 11% or less of chance of existing and also stereochemical constraints with residues Gln14, Arg15, Ser33 and Gly228. From these 19 possible orientations, 14 seem to be in a certain orientation that would allow for the establishment of hydrogen bonds, namely with residues Tyr35, Gly228, Cys173, Asp16 and Asp174.

It should be noted that a low probability like the ones described before, only informs about how likely is to have a structural change in these cases. Even though it would not be likely to have the structure shown in Figures 23 and 24, it would be very probable that the structural changes caused by the mutations might have occurred in the same places as the clashes. The fact that the rotamers' probabilities observed for the substitution of Ser34 by an aspartate are lower than the ones observed for the substitution of Ser33 by an aspartate, indicate that the structure of the mutant S34D would be more affected by the mutation than the structure of the mutant S33D when compared with the wild type protein structure. That higher probability of causing structural changes combined with the fact that Ser34 is not oriented towards the entrance of the product escape route seems to indicate that the impact of the S34D mutation could be more related to the structure stabilisation and not so much to the partial blocking of the products' escape route. Thus, the difference of activities observed for the mutant S33D when compared to the wild type protein could be attributed to a slight difference in hydrogen bonds, related to the active site or not, or due to partial blocking of the products escape route, while the difference observed for mutant S34D would be mainly caused by a structural change that does not directly involve the active site or product's escape route, even though an indirect involvement cannot be discarded.

However, in order to verify these hypotheses and take further conclusions, it would be necessary to obtain the crystallographic structure and/or carry out a minimisation of the energy of protein structure, in order to obtain structures that could better approximate the reality and, then, be able to observe the impact of each mutation in the protein structure. Also, it would be important to analyse the protein´s dynamics since mutations far apart from an active site may affect the overall protein dynamics through long-range effects.

6. Conclusions and future perspectives

In this experimental work it was possible to characterise FlRd wild type and the mutants proposed in the beginning of this experimental work. The comparison between the wild type protein and the mutants did not show any significant alteration in the biochemical properties of the wild type protein since the iron and flavin incorporation, quaternary structure, UV-visible spectra and melting temperature were very similar.

However, kinetically, even though the activity towards two of the three substrates (molecular oxygen and hydrogen peroxide) was similar, it was possible to observe a significant decrease of activity towards the preferential substrate (nitric oxide). This decrease may be due to structural modifications and different electrostatic effects near the mutation's positions that somehow affect the substrate/product entrance/exit of the active site, which is more noticeable in conditions of faster turnover rates as when the protein is reducing NO to N_2O.

Even though enlightening results were obtained in this experimental work, further studies should be carried out in order to fully understand the role played by serines 33 and 34 in the conserved motif near the active site. These further studies should include the determination of the mutants' structures by X-ray crystallography (not achieved in this experimental work) so that it can be possible to hypothesise about observable structural changes, in case they exist, and also the determination of the reduction potentials of the rubredoxin and diiron centres, as well as the FMN co-factor potential, to understand if and how this mutation would affect the electron transfer process.

7. References

1. Holland, H. D. The oxygenation of the atmosphere and oceans. *Philos. Trans. R. Soc. B Biol. Sci.* **361**, 903–915 (2006).
2. Lehninger, A. L, 2004, Principles of Biochemistry, 690-722, 4th edition, W. H. Freeman and Company, New York
3. Stryer, L., 1988, Biochemistry, 400, 3rd edition, W. H. Freeman and Company, New York
4. Imlay, J. A. Cellular Defenses against Superoxide and Hydrogen Peroxide. *Annu. Rev. Biochem.* **77**, 755–776 (2008).
5. Wink, D. A. *et al.* Nitric oxide and redox mechanisms in the immune response. *J. Leukoc. Biol.* **89**, 873–891 (2011).
6. Fang, F. C. Antimicrobial reactive oxygen and nitric oxide species: concepts and controversies. *Nat. Rev. Microbiol.* **2**, 820–832 (2004).
7. Yang, Y., *et al.* S. Reactive Oxygen Species in the Immune System. *Int. Rev. Immunol.* 1–22 (2012).
8. MacMicking, *et al*. Nitric oxide and macrophage function. *Annu. Rev. Immunol.* **15**, 323–350 (1997).
9. Lundberg, J. O., & Weitzberg, E. Biology of nitrogen oxides in the gastrointestinal tract. *Gut*, **62**(4), 616–629 (2012).
10. Toledo Jr, J. C. & Augusto, O. Connecting the Chemical and Biological Properties of Nitric Oxide. *Chem. Res. Toxicol.* **25**, 975–989 (2012).
11. Winterbourn, C. C. Reconciling the chemistry and biology of reactive oxygen species. *Nat. Chem. Biol.* **4**, 278–286 (2008).
12. Vázquez-Torres, A. Redox Active Thiol Sensors of Oxidative and Nitrosative Stress. *Antioxid. Redox Signal.* **17**, 1201–1214 (2012).
13. Crack, J., Green, J. & Thomson, A. J. Mechanism of Oxygen Sensing by the Bacterial Transcription Factor Fumarate-Nitrate Reduction (FNR)*. *J. Biol. Chem.* **279**, 9278–9286 (2004).
14. D'Autréaux, B., *et al*. A non-haem iron centre in the transcription factor NorR senses nitric oxide. *Nature* **437**, 769–772 (2005).
15. Maxwell, D. P., *et al*. The alternative oxidase lowers mitochondrial reactive oxygen production in plant cells. *Proc. Natl. Acad. Sci.* **96**, 8271–8276 (1999).
16. Mcdonald, A. E., *et al*. Prokaryotic orthologues of mitochondrial alternative oxidase and plastid terminal oxidase. *Plant Mol. Biol.* **53**, 865–876 (2003).
17. Liu, L. *et al*. A metabolic enzyme for S-nitrosothiol conserved from bacteria to humans. *Nature* **410**, 490–494 (2001).

18. Bryk, R., *et al*. Peroxynitrite reductase activity of bacterial peroxiredoxins. *Nature* **407**, 211–215 (2000).
19. Chen, L. *et al.* Rubredoxin Oxidase, a new flavo-hemo-protein, is the site of oxygen reduction to water by the 'strict anaerobe' *Desulfovibrio gigas*. *Biochem. Biophys. Res. Commun.* **193**, 100–105 (1993).
20. Folgosa, F., *et al*. Diversity and complexity of flavodiiron NO/O_2 reductases. *FEMS Microbiol. Lett.* **365**, 1–8 (2018).
21. Martins, M. C. *et al.* Free Radical Biology and Medicine How superoxide reductases and flavodiiron proteins combat oxidative stress in anaerobes. *Free Radic. Biol. Med.* **140**, 36-60 (2019).
22. Romão, C. V., *et al*. The dual function of flavodiiron proteins : oxygen and/or nitric oxide reductases. *J. Biol. Inorg. Chem.* **21**, 39–52 (2016).
23. Gomes, C. M., *et al*. A Novel Type of Nitric oxide Reductase. *J. Biol. Chem.* **277**, 25273–25276 (2002).
24. Victor, B. L., *et al*. Dioxygen and nitric oxide pathways and affinity to the catalytic site of rubredoxin : oxygen oxidoreductase from *Desulfovibrio gigas*. *J. Biol. Inorg. Chem.* **14**, 853–862 (2009).
25. Gonçalves, V. L. *et al.* Flavodiiron Oxygen Reductase from *Entamoeba histolytica*. *J. Biol. Chem.* **289**, 28260–28270 (2014).
26. Folgosa, F., *et al*. The multidomain flavodiiron protein from Clostridium difficile 630 is an NADH : oxygen oxidoreductase. *Nat. Sci. Reports* **8**, 1–13 (2018).
27. Kint, N. *et al.* How the Anaerobic Enteropathogen *Clostridioides difficile* tolerates low O_2 tensions. *Mol. Biol. Physiol.* **11**, 1–17 (2020).
28. Seedorf, H., *et al*. F420H2 oxidase (FprA) from *Methanobrevibacter arboriphilus*, a coenzyme F420-dependent enzyme involved in O_2 detoxification, *Arch. Microbiol.* **182,** 126–137 (2004).
29. Seedorf, H., *et al*. Structure of coenzyme F420H2 oxidase (FprA), a di-iron flavoprotein from methanogenic Archaea catalyzing the reduction of O_2 to H_2O, *FEBS J.* **274**, 1588–1599 (2007).
30. Wasserfallen, A., *et al*. A family of flavoproteins in the domains Archaea and Bacteria, *Eur. J. Biochem*. **254** 325–332 (1998).
31. Smutna, T., *et al.* Flavodiiron protein from *Trichomonas vaginalis* hydrogenosomes: the terminal oxygen reductase, *Eukaryot. Cell* **8** 47–55 (2009).
32. Di Matteo, A., *et al*. The O_2-scavenging flavodiiron protein in the human parasite *Giardia intestinalis*, *J. Biol. Chem.* **283** 4061–4068 (2008).
33. Vicente, J.B., *et al*. A detoxifying oxygen reductase in the anaerobic protozoan *Entamoeba histolytica*, *Eukaryot. Cell* **11** 1112–1118 (2012).

34. Silaghi-Dumitrescu, R., *et al*. A flavodiiron protein and high molecular weight rubredoxin from *Moorella thermoacetica* with nitric oxide reductase activity, *Biochemistry* **42** 2806–2815 (2003).
35. Kawasaki, S., *et al.* Identification of O_2-induced peptides in an obligatory anaerobe, *Clostridium acetobutylicum, FEBS Lett*. **571** 21–25 (2004).
36. Helman, Y., *et al.* Genes Encoding A-Type Flavoproteins Are Essential for Photoreduction of O_2 in *Cyanobacteria*. *Curr. Biol.* **13**, 230–235 (2003).
37. Allahverdiyeva, Y., *et al*. Cyanobacterial Oxygenic Photosynthesis is Protected by Flavodiiron Proteins. *Life* **5**, 716–743 (2015).
38. Ilík, P. *et al.* Rapid report Alternative electron transport mediated by flavodiiron proteins is operational in organisms from cyanobacteria up to gymnosperms. *New Pathol.* **214**, 967–972 (2017).
39. Frazão, C., *et al*. Structure of a dioxygen reduction enzyme from *Desulfovibrio gigas*. *Nat. Struct. Biol.* **7**, 1041–1045 (2000).
40. Romão, C. V, *et al*. Structure of *Escherichia coli* Flavodiiron Nitric Oxide Reductase. *J. Mol. Biol.* **428**, 4686–4707 (2016).
41. Cabeza, M. S., *et al*. New enzymatic pathways for the reduction of reactive oxygen species in *Entamoeba histolytica*. *BBA - Gen. Subj.* **1850**, 1233–1244 (2015).
42. Blomberg, L. M., Blomberg, M. R. A. & Siegbahn, P. E. M. Theoretical study of the reduction of nitric oxide in an A-type flavoprotein. *J. Biol. Inorg. Chem.* **12**, 79–89 (2006).
43. Petoukhov, M. V., *et al.* Quaternary Structure of Flavorubredoxin as Revealed by Synchrotron Radiation. *Structure* **16**, 1428–1436 (2008).
44. Meyer, J. & Moulis, J. Rubredoxin. *Handb. Met.* 1–13 (2006).
45. Sheridan, W. G., *et al*. Intraoperative Tissue Oximetry in the Human Gastrointestinal Tract. *Am. J. Surg.* **159**, 314–319 (1990).
46. Chen, Z. & Cole, P. A. ScienceDirect Synthetic approaches to protein phosphorylation. *Curr. Opin. Chem. Biol.* **28**, 115–122 (2015).
47. Fortune, W. B. & Mellon, M. G. Determination of Iron with o-Phenanthroline. *Ind. Engeneering Chem.* **15**, 60–64 (1938).
48. Chapman, S. K. & Reid, G. A. Flavoprotein protocols. in *Methods in Molecular Biology* 1–7 (1999).
49. Kruger, N. J. The Bradford Method For Protein Quantitation. in *The Protein Protocols Handbook* 17–24 (2009).

50. Greenfield, N. J. Using circular dichroism collected as a function of temperature to determine the thermodynamics of protein unfolding and binding interactions. *Nat. Protoc.* **1**, 2527–2535 (2009).
51. Lee, S., Kim, J., Han, S. & Park, C. Recognition and Unfolding of c - MYC and Telomeric G - Quadruplex DNAs by the RecQ C - Terminal Domain of Human Bloom Syndrome Helicase. *ACS Omega*, **5**, 14513–14522 (2020).
52. Gnaiger, E. The Oxygraph for High-Resolution Respirometry (HRR). *Oroboros instruments*. 1–18 (2011). Read on October 19th, 2020. Available at: https://wiki.oroboros.at/images/7/76/MiPNet06.01_O2k-Overview.pdf.
53. Hussein, M. & Najm, H. Data in Brief Data supporting the spectrophotometric method for the estimation of catalase activity. *Data Br.* **6**, 194–199 (2016).
54. Panda, C., *et al*. Catalytic signal amplification using [Fe(III)(biuret-amide)]-mesoporous silica nanoparticles: visual cyanide detection. *R. Soc. Chem.* **49**, 2216–2218 (2013).
55. Bernofskys, C. & Wanda, S. C. Formation of Reduced Nicotinamide Adenine Dinucleotide Peroxide. *J. Biol. Chem.* **257**, 6809–6817 (1982).
56. Instruments, W. P. Apollo 4000: Instruction manual. 1–74 (2003). Read on October 19th, 2020. Available at: https://www.wpiinc.com/media/wysiwyg/pdf/apollo-4000-im-061506.pdf.
57. Ameh, E. S. A review of basic crystallography and x-ray diffraction applications. *Int. J. Adv. Manuf. Technol.* **105**, 3289–3302 (2019).
58. Shi, Y. A Glimpse of Structural Biology through X-Ray Crystallography. *Cell* **4**, 995–1014 (2014).
59. Roessler, M. M. & Salvadori, E. Principles and applications of EPR spectroscopy in the chemical sciences. *R. Soc. Chem.* **47**, 2534–2553 (2018).
60. Gomes, C. M., *et al*. Spectroscopic Studies and Characterization of a Novel Electron-Transfer Chain from *Escherichia coli* Involving a Flavorubredoxin and Its Flavoprotein Reductase Partner. *Biochemistry* **39**, 16230–16237 (2000).
61. Vicente, J. B. & Teixeira, M. Redox and Spectroscopic Properties of the *Escherichia coli* Nitric Oxide-detoxifying System Involving Flavorubredoxin and Its NADH-oxidizing Redox Partner *. *J. Biol. Chem.* **280**, 34599–34608 (2005).
62. Vicente, B., *et al*. Biochemical, Spectroscopic, and Thermodynamic Properties of Flavodiiron Proteins. in *Methods in Enzymology* **437**, 21–45 (2008).
63. Hunter, T. Why nature chose phosphate to modify proteins. *Philos. Trans. R. Soc. B* **367**, 2513–2516 (2012).
64. Pettersen, E. F. *et al.* UCSF Chimera: A Visualization System for Exploratory Research and Analysis. *J. Comput. Chem.* **25**, 1605–1612 (2004).

8. Appendices

Appendix 8.2 – Liquide LB medium composition.

Reagent	Mass/ Volume
Triptone	10 g
Yeast Extract	5 g
NaCl	10 g
H_2O Milli-Q	Up to 1000 mL

Appendix 8.1 –LB agar medium composition.

Reagent	Mass/ Volume
Triptone	3 g
Yeast Extract	1.5 g
NaCl	3 g
Agar	6
H_2O Milli-Q	Up to 300 mL

Appendix 8.3 – M9 Salts composition.

Reagent	Mass/ Volume
$Na_2HPO.7H_2O$	128 g
KH_2PO_4	30 g
NH_4Cl	10 g
NaCl	5 g
H_2O Milli-Q	Up to 2000 mL

Appendix 8.4 – M9 Medium composition.

Reagent	Volume
M9 Salts (5x)	400 mL
1 M $MgSO_4$	4 mL
5 M $CaCl_2$	0.04 mL
1 M Glucose	40 mL
0.1 M $FeCl_2$	2 mL + 2 mL (together with IPTG)
Kanamycin (50 mg/mL)	200 µL
H_2O Milli-Q	Up to 2000 mL

Appendix 8.5 – SDS-PAGE buffers

Appendix 8.5.1 – Solution I used in SDS-PAGE gel.

Reagent	Mass/ Volume
1.5 M Tris Base	18.2 g
Concentrated HCl	Until pH 8.8
SDS	0.3 g
dH_2O	Up to 100 mL

Appendix 8.5.2 – Solution II used in SDS-PAGE gel.

Reagent	Mass/ Volume
0.5 M Tris Base	6.06 g
Concentrated HCl	Until pH 6.8
SDS	0.4 g
dH_2O	Up to 100 mL

Appendix 8.5.3 – Sample buffer for sample preparation for SDS-PAGE gels.

Reagent	Mass/ Volume
Solution II	5 mL
SDS	0.8 g
β-mercaptoethanol	1 mL
Glycerol	2 mL
Bromophenol blue	4 mg
dH_2O	Up to 2000 mL

Appendix 8.5.4 – SDS-PAGE gel composition.

RESOLVING GEL		
Reagent	Volume (µL)	
	12.5 %	15 %
Solution I	2500	2500
Acrylamide/Bisacrylamide (30:0.8)	4166	5000
dH_2O	3334	2500
10% APS	40	
β-mercaptoethanol	10	

STACKING GEL	
Reagent	Volume (µL)
Solution II	1250
Acrylamide/Bisacrylamide (30:0.8)	650
dH_2O	3050
10% APS	40
β-mercaptoethanol	10

Appendix 8.5.5 – Coomassie Brilliant Blue protein staining.

Reagent	Mass/ Volume
Coomassie Blue R-250	1 g
Glacial acetic acid	15 mL
Methanol	90 mL
dH_2O	Up to 200 mL

Appendix 8.5.6 – Distaining solution for Coomassie stained SDS-PAGE gels.

Reagent	Volume
Glacial acetic acid	75 mL
Methanol	450 mL
dH_2O	Up to 1000 mL

Appendix 8.6 – TAE buffer stock solution for electrophoresis in agarose gel

Reagent	Mass/ Volume
Tris Base	242 g
Disodium EDTA	18.61 g
Acetic Acid	59.96 g
dH_2O	Up to 1000 mL

In order to prepare TAE buffer 1x, used in the agarose gels, the stock solution was diluted 25x.

Appendix 8.7 – Gel filtration chromatogram of FlRd mutants (S33D and S34D) corrected for the void volume marker (Blue dextran) and calibration curve. **S33D** – Full blue line; **S34D** – Full yellow line.

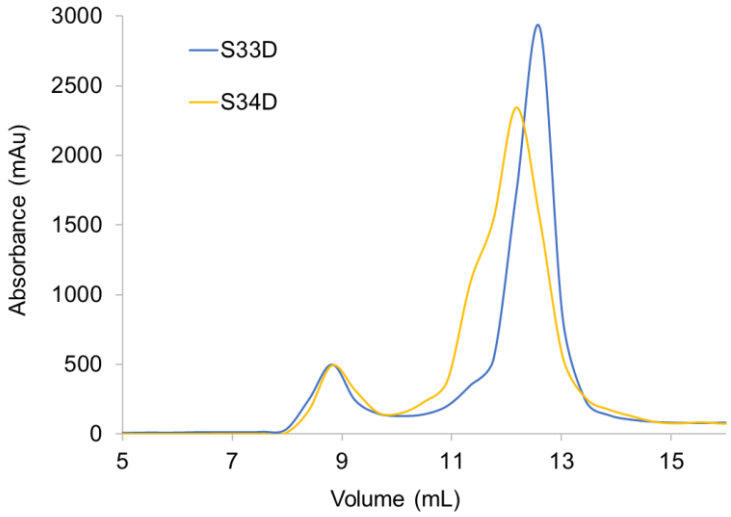

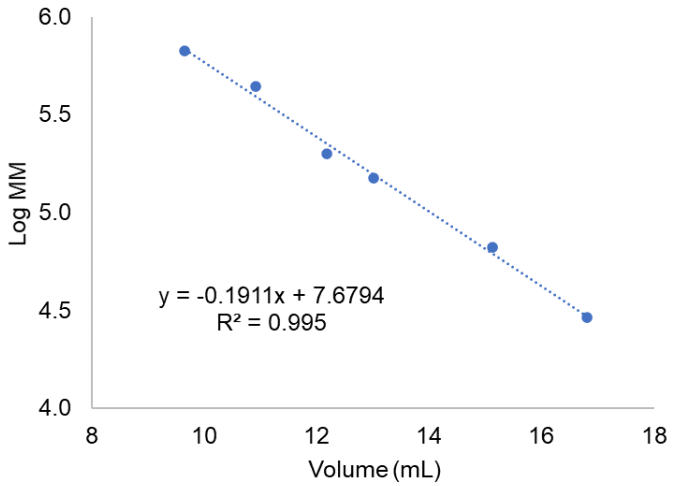

Appendix 8.8 – Composition of the set of buffers tested in thermofluor assay.

	1	2	3	4	5	6	7	8	9	10	11	12
A	100 mM Sodium Acetate pH 4.5	100 mM Sodium Citrate pH 5.0	100 mM Sodium Citrate pH 5.5	100 mM Potassium Phosphate pH 6.0	100 mM MES pH 6.2	100 mM Sodium Phosphate pH 6.5	100 mM Sodium Cacodylate pH 6.5	100 mM ADA pH 6.5	100 mM Bis-Tris Propane pH 6.5	100 mM Sodium Phosphate pH 7.0	100 mM HEPES pH 7.0	100 mM MOPS pH 7.0
B	100 mM Ammonium Acetate pH 7.0	100 mM Tris pH 7.4	100 mM Potassium Phosphate pH 7.5	100 mM Sodium Acetate pH 7.5	100 mM MES pH 7.5	100 mM Imidazole pH 8.0	100 mM Tricine pH 8.0	100 mM Tris pH 8.0	100 mM HEPES pH 8.5	100 mM Tris pH 8.5	100 mM Bicine pH 9.0	100 mM CHES pH 9.5
C	100 mM Sodium Acetate pH 4.5, 150 mM NaCl	100 mM Sodium Citrate pH 5.0, 150 mM NaCl	100 mM Sodium Citrate pH 5.5, 150 mM NaCl	100 mM Potassium Phosphate pH 6.0, 150 mM NaCl	100 mM MES pH 6.2, 150 mM NaCl	100 mM Sodium Phosphate pH 6.5, 150 mM NaCl	100 mM Sodium Cacodylate pH 6.5, 150 mM NaCl	100 mM ADA pH 6.5, 150 mM NaCl	100 mM Bis-Tris Propane pH 6.5, 150 mM NaCl	100 mM Sodium Phosphate pH 7.0, 150 mM NaCl	100 mM HEPES pH 7.0, 150 mM NaCl	100 mM MOPS pH 7.0, 150 mM NaCl
D	100 mM Ammonium Acetate pH 7.0, 150 mM NaCl	100 mM Tris pH 7.4, 150 mM NaCl	100 mM Potassium Phosphate pH 7.5, 150 mM NaCl	100 mM Sodium Acetate pH 7.5, 150 mM NaCl	100 mM MES pH 7.5, 150 mM NaCl	100 mM Imidazole pH 8.0, 150 mM NaCl	100 mM Tricine pH 8.0, 150 mM NaCl	100 mM Tris pH 8.0, 150 mM NaCl	100 mM HEPES pH 8.5, 150 mM NaCl	100 mM Tris pH 8.5, 150 mM NaCl	100 mM Bicine pH 9.0, 150 mM NaCl	100 mM CHES pH 9.5, 150 mM NaCl
E	100 mM Sodium Acetate pH 4.5, 250 mM NaCl	100 mM Sodium Citrate pH 5.0, 250 mM NaCl	100 mM Sodium Citrate pH 5.5, 250 mM NaCl	100 mM Potassium Phosphate pH 6.0, 250 mM NaCl	100 mM MES pH 6.2, 250 mM NaCl	100 mM Sodium Phosphate pH 6.5, 250 mM NaCl	100 mM Sodium Cacodylate pH 6.5, 250 mM NaCl	100 mM ADA pH 6.5, 250 mM NaCl	100 mM Bis-Tris Propane pH 6.5, 250 mM NaCl	100 mM Sodium Phosphate pH 7.0, 250 mM NaCl	100 mM HEPES pH 7.0, 250 mM NaCl	100 mM MOPS pH 7.0, 250 mM NaCl, 250 mM NaCl
F	100 mM Ammonium Acetate pH 7.0, 250 mM NaCl	100 mM Tris pH 7.4, 250 mM NaCl	100 mM Potassium Phosphate pH 7.5, 250 mM NaCl	100 mM Sodium Acetate pH 7.5, 250 mM NaCl	100 mM MES pH 7.5, 250 mM NaCl	100 mM Imidazole pH 8.0, 250 mM NaCl	100 mM Tricine pH 8.0, 250 mM NaCl	100 mM Tris pH 8.5, 250 mM NaCl	100 mM HEPES pH 8.5, 250 mM NaCl	100 mM Tris pH 8.5, 250 mM NaCl	100 mM Bicine pH 9.0, 250 mM NaCl	100 mM CHES pH 9.5, 250 mM NaCl
G	100 mM Sodium Acetate pH 4.5, 500 mM NaCl	100 mM Sodium Citrate pH 5.0, 500 mM NaCl	100 mM Sodium Citrate pH 5.5	100 mM Potassium Phosphate pH 6.0, 500 mM NaCl	100 mM MES pH 6.2, 500 mM NaCl	100 mM Sodium Phosphate pH 6.5, 500 mM NaCl	100 mM Sodium Cacodylate pH 6.5, 500 mM NaCl	100 mM ADA pH 6.5, 500 mM NaCl	100 mM Bis-Tris Propane pH 6.5, 500 mM NaCl	100 mM Sodium Phosphate pH 7.0, 500 mM NaCl	100 mM HEPES pH 7.0, 500 mM NaCl	100 mM MOPS pH 7.0, 500 mM NaCl
H	100 mM Ammonium Acetate pH 7.0, 500 mM NaCl	reference	100 mM Potassium Phosphate pH 7.5, 500 mM NaCl	100 mM Sodium Acetate pH 7.5, 500 mM NaCl	100 mM MES pH 7.5, 500 mM NaCl	100 mM Imidazole pH 8.0, 500 mM NaCl	100 mM Tricine pH 8.0, 500 mM NaCl	100 mM Tris pH 8.0, 500 mM NaCl	100 mM HEPES pH 8.5, 500 mM NaCl	100 mM Tris pH 8.5, 500 mM NaCl	100 mM Bicine pH 9.0, 500 mM NaCl	100 mM CHES pH 9.5, 500 mM NaCl